REPORT DOCUMENTATION PAGE

AFRL-SR-BL-TR-98-

0058

urces, if this erson

1. AGENCY USE ONLY (Leave blank)	2. REPORT DATE	3. REPORT TYPE AND DATES COVERED
	December 1997	Final Technical: 15 OCT 93 to 14 OCT 97

4. TITLE AND SUBTITLE

Research on XUV Lasers and Applications

5. FUNDING NUMBERS

G F49620-94-1-0017
PR 2301/BS
FQ8671-9400088

6. AUTHOR(S)

Dr. James F. Young
Professor, Electrical & Computer Engineering

7. PERFORMING ORGANIZATION NAME(S) AND ADDRESS(ES)

Rice University
Office of Sponsored Research
P.O. Box 2692
Houston, TX 77252

8. PERFORMING ORGANIZATION REPORT NUMBER

9. SPONSORING/MONITORING AGENCY NAME(S) AND ADDRESS(ES)

AFOSR/NE
Dr. Howard R. Schlossberg
110 Duncan Avenue, Suite B115
Bolling AFB, DC 20332-0001

10. SPONSORING/MONITORING AGENCY REPORT NUMBER

11. SUPPLEMENTARY NOTES

12a. DISTRIBUTION/AVAILABILITY STATEMENT

Unlimited

12b. DISTRIBUTION CODE

13. ABSTRACT *(Maximum 200 words)*

The focus of this program was the development of extreme ultraviolet (XUV) sources, and their application to scientific problems. Laser development concentrated on the laboratory-scale Xe Auger laser at 109 nm; we also developed broad bandwidth incoherent sources. The primary application area was the development of high resolution, microscopic imaging techniques. Such techniques should have a number of applications, and be particularly useful in the life sciences. This report presents a summary of the program accomplishments, presentations, and copies of papers published.

14. SUBJECT TERMS

Imaging; Ultraviolet; Vacuum Ultraviolet; Laser.

15. NUMBER OF PAGES

16. PRICE CODE

17. SECURITY CLASSIFICATION OF REPORT	18. SECURITY CLASSIFICATION OF THIS PAGE	19. SECURITY CLASSIFICATION OF ABSTRACT	20. LIMITATION OF ABSTRACT
UNCLASSIFIED	UNCLASSIFIED	UNCLASSIFIED	

Research on XUV Lasers and Applications

AFOSR Grant F49620–94–1–0017
Final Technical Report

James. F. Young
Principal Investigator & Professor,

Department of Electrical and Computer Engineering,
Rice University, P.O. Box 1892, Houston, TX 77251
Phone: (713) 527–4721; FAX: (713) 524–5237; young@rice.edu

15 October 1993 — 14 October 1997

1 Introduction

The focus of this program was the improved understanding of XUV sources, application of that knowledge to develop improved source characteristics and accessibility, and the use of those sources for innovative and practical applications. This work built upon the the results of our previous grant, AFOSR–90–0257. Source development concentrates on the laboratory-scale Xe Auger laser near 100 nm and broad bandwidth laser produced plasmas. The current application area is the development of microscopic imaging techniques, particularly for the life sciences. In addition, at the end this program supported work on a new technique for optical communications networks, which is being continued with partial support from the follow-on grant AFOSR F49620–97–1–0349, which began 01 May 1997.

The progress and results of this program have been documented in previous yearly Technical Progress Reports, the most recent covering the period through 31 July 1997, only 10 weeks ago. A cummulative summary of accomplishments is presented below. Most importantly, significant results have been reported in the scientific literature and in presentations at conferences; these are also listed below, and copies of articles are attached to this report.

2 Personnel Supported

Senior Personnel

1. Dr. James F. Young, Principle Investigator and Professor; Summer salary only.
2. Dr. Christopher Bonang, Research Scientist.
3. Dr. Csaba Tòth, Research Scientist.

Students

1. Tracy Sharp, Ph.D. 1993.
2. Lim Nguyen, Ph.D. 1996, participant in the Palace Knight program at Phillips Laboratory.
3. J. Wu, M.S. 1994.
4. K. Dillon, M.S. July 1996.
5. Y. Guo, M.S. 1996, in Ph.D. program.
6. H. M. Duiker, graduate student.
7. I. Ferincz, visiting Ph.D. student from JATE university, Szeged, Hungary.
8. Tasshi Dennis, M.S. 1995, Ph.D. expected summer 1998.
9. M. Gross, undergraduate research assistant.
10. Amy W. Horton, undergraduate research assistant.

3 Cummulative Summary of Accomplishments

- Constructed a broad bandwidth, laser-produced plasma VUV source for film and sample investigations, and for contact printing; a number of innovations reduce target debris significantly while maintaining high flux levels.
- Measured PMMA response characteristics (depth versus exposure energy) for exposures in the 60 to 130 nm spectral range; this data is critical for image reconstruction and was not previously available.
- Determined PMMA absorption coefficient in the VUV using a development model; validated exposure/development models are useful in predicting PMMA and other polymer film response in new spectral regions.

- Demonstrated that atomic force microscope readout of exposed PMMA film provides improved sensitivity and precision over previous methods; despite shallow penetration of light into the film, sufficient grey scale or intensity resolution (greater than 8 levels) is available for imaging.
- Measured gain in the ionic excimer $Cs^{2+}F^{-}$, the first of a new class of short wavelength lasers that could prove useful for imaging when further developed.
- Developed and characterized a laboratory-scale, VUV laser source for imaging; the Xe^{2+} Auger laser provides up to 1 μJ pulses at 109 nm (11.5 eV) and operates at 6 Hz pumped by a commercial laser system.
- Investigated the efficiency of various laser-produced plasma target materials for pumping the Xe Auger laser; gold produces twice the laser output as stainless steel, reducing exposure times.
- Recorded interference fringes on PMMA using the Xe 109 nm laser; we are using the fringe visibility to characterize the source coherence.
- Imaged biological cells on PMMA using both our laser-produced plasma source and the Xe^{2+} laser; regions of different contrast are evident.
- Recorded simple holograms of test spheres using the Xe^{2+} laser.
- Initiated a collaboration with Colorado State University to make exposures of biological cells at shorter wavelengths: $\sim$ 49 nm.
- Performed theoretical calculations showing that with proper code design, time-domain bipolar-equivalent encoding/decoding can produce the same performance in multiuser optical channels as the well developed radio-frequency spread spectrum technique.
- Performed theoretical calculations showing that spectral code division multiplexing can cancel the effects of four wave mixing to first order in point to point communications channels.
- Continued construction of an all-fiber test bed for our CDMA measurements.

Related Publications and Presentations

- I. E. Ferincz, C. Tóth, and J. F. Young, "Resist Characteristics of Poly(Methyl Methacrylate) at Vacuum Ultraviolet Wavelengths for High Resolution Imaging," *J. Vac. Sci. Technol. B*, Vol. 15, No. 4, pp. 828–832, 1997.
- T. Dennis, H. M. Duiker, J. Wu, C. Tóth, and J. F. Young, "Comparison of Laser-Produced Plasma Target Materials for Pumping the 109 nm Xe^{2+} Auger Laser," *IEEE J. Selected Topics in Quantum Electronics*, Vol. 1, pp. 867–871, 1995.

- J. F. Young, H. M. Duiker, I. Ferincz, and T. Dennis, "Vacuum Ultraviolet Optical Microscopy," *SPIE Proceedings*, vol. 2524, pp. 201–207, 1995.

- J. F. Young, "Short Wavelength Microscopy," *IEEE Lasers and Electo-Optics Society Newsletter*, Vol. 8, No. 3, pp. 1–15, June 1994.

- J. F. Young, "Laser-Produced Plasmas as Short Wavelength, Incoherent Optical Sources," in *Atomic, Molecular, and Optical Physics: Electromagnetic Radiation* F. B. Dunning and R. G. Hulet, eds., Chapter 1 (Academic Press, 1997).

- T. S. Clement, C. Tóth, J. Wu, and J. F. Young, "A Reasonably Practical XUV Laser for Applications," *IEEE Journal of Quantum Electronics*, vol. 30, pp. 2136–2140, 1994.

- C. Tóth, J. F. Young, and R. Sauerbrey, "Optical Gain in the Ionic Excimer $Cs^{2+}F^{-}$ Excited by Soft X-Rays from a Laser-Produced Plasma," *Optics Letters*, vol. 18, pp. 2120–2122, 1993.

- Y. Guo, B. Aazhang, and J. F. Young, "Wavelength Encoding to Reduce Four-Wave Mixing Crosstalk in Multi-Wavelength Channels," IEEE Lasers and Electro-Optics Society Annual Meeting, San Francisco, CA, November 1997.

- T. Dennis, B. Aazhang, and J. F. Young. "Demonstration of All-Optical CDMA with Bipolar Codes," IEEE Lasers and Electro-Optics Society Annual Meeting, San Francisco, CA, November 1997.

- T. Dennis, L. Nguyen, B. Aazhang, and J. F. Young, "Experimental Demonstration of Bipolar Codes for Direct Detection Multi-User Optical Communication," IEEE/LEOS 1996 Summer Topical Meeting: Broadband Optical Networks–Enabling Technologies and Applications, Keystone, CO, August 1996.

- Cs. Tóth, I. Ferincz, and J. F. Young, "Study of the Spatial Coherence of the VUV Xe^{2+} Auger Laser by Holographic Imaging," IEEE Lasers and Electro-Optics Society Annual Meeting, Boston, MA, November 1996.

- A. W. Horton, Cs. Tóth, I. E. Ferincz, and J. F. Young, "High Resolution Contact Imaging in the Vacuum Ultraviolet," Tenth Annual RQI Summer Research Colloquium, Houston, TX, August 1996.

- T. Dennis, H. M. Duiker, J. Wu, C. Tóth, and J. F. Young, "Comparison of Laser-Produced Plasma Target Materials for Pumping the 109 nm Xe^{+2} Auger Laser," IEEE LEOS Eighth Annual Meeting, San Francisco, CA, October 1995.

- Cs. Tóth, R. Sauerbrey, and J. F. Young, "Observation of Gain in the Ionic Excimer $Cs^{2+}F^{-}$," CLEO/Europe-EQEC '94, Amsterdam, Netherlands, August 1994 (Invited).

- J. F. Young, "Holographic Microscopy at 109 nm," Future Prospects for UV and VUV Lasers III, Santa Barbara, CA, February 1994 (Invited).

- Cs. Tóth, R. Sauerbrey, and J. F. Young, "Gain at 185 nm in the Ionic Excimer $Cs^{2+}F^{-}$," Future Prospects for UV and VUV Lasers III, Santa Barbara, CA, February 1994.

4 Relationship to Other Programs and Support

The imaging applications portion of this work was jointly supported by the National Science Foundation; the optical communications work was jointly supported by the Texas Advanced Technology Program.

File: ~/doc/grants/AF_93/af93-final.tex.

Imaging characteristics of poly(methyl methacrylate) at vacuum ultraviolet wavelengths

I. E. Ferincz,[a] Cs. Tóth,[b] and J. F. Young[c]
Department of Electrical and Computer Engineering and the Rice Quantum Institute, Rice University, Houston, Texas 77251

(Received 11 October 1996; accepted 9 May 1997)

We report the depth versus exposure characteristics of poly(methyl methacrylate) (PMMA) in the vacuum ultraviolet (VUV) region from 59 to 128 nm. Calculated absorption coefficients of the PMMA are also presented. The depth of the features on the PMMA were in the range of 20–80 nm created by 1–50 mJ cm^{-2} exposures and were measured with an atomic force microscope (AFM). We found that the AFM can reliably measure depth differences of only 2 nm. The sensitivity of the AFM permits exposures to be reduced for high resolution microscopy and holography even in the case of highly absorbing films. © *1997 American Vacuum Society.* [S0734-211X(97)12404-0]

I. INTRODUCTION

Microscopy using contact printing or holography requires a well characterized, high resolution recording film. One of the earliest and best characterized electron and x-ray resists is poly(methyl methacrylate) (PMMA).[1–3] In contrast, however, to lithography applications — where the full removal of the resist is desirable in the exposed areas — contact imaging and holography require a resist with vertical (depth) resolution. The attainability of a ''grey-scale'' pattern in the resist is important in these applications for reliable and reproducible mapping of the light intensity in a wide exposure range. In the soft x-ray region, microscopy using PMMA as a resist material is well developed.[4] In PMMA, a positive resist, bonds are broken by incident short wavelength radiation, decreasing the average molecular weight of the long-chain molecules. This increases the solubility of the resist in a suitable solvent, resulting in a pattern of surface heights corresponding to the exposure. The surface pattern can be measured by a scanning[5] or transmission electron microscope,[6,7] but an atomic force microscope (AFM) provides more reliable quantitative data.[8,9]

Vacuum ultraviolet (VUV) microscopy has the potential to supplement x-ray and electron microscopy, because the contrast mechanism is quite different. VUV radiation interacts with the outer valance electrons and molecular absorption is sensitive to composition and structure. In addition, several reasonably practical incoherent and coherent sources exist in the 80–130 nm region. However, almost no studies have been made of PMMA, or other films, for VUV imaging. While there are lithography studies in the 110–260 nm region,[10–12] this information is only partly relevant since the requirements of lithography are quite different from imaging. For lithography, the critical parameter is the exposure required to completely remove the film; imaging, however, requires quantitative knowledge of the response function and a reasonable dynamic range, or intensity level resolution. The relationship between exposure and surface height is generally poorly known even for common photoresists. Basic and important optical constants, such as absorption coefficient at VUV wavelengths are also lacking.

In this work we will present the depth-exposure characteristics of PMMA in the 59–128 nm spectral range, for exposure values of 1–50 mJ cm^{-2}. The surface depths were measured with an AFM and were in the range of 2–80 nm. Since the AFM can reliably measure surface height differences of only 2 nm, very low exposures can be used even at wavelengths that are highly absorbing. We have used our depth versus exposure data to calculate the VUV absorption coefficients of PMMA using a simple model for exposure and dissolution.

II. EXPERIMENTAL DESCRIPTION

A. Preparation and development of the PMMA resist

The samples for exposure were 12.5 mm diameter polished glass disks spin coated with PMMA. The resist was a commercial solution of 4% PMMA (molecular weight of 950 000) in chlorobenzene.[13] The top surface of the substrate was flooded with the PMMA solution and then spun at 5000 rpm for 25 s. A second layer of PMMA was spun over the first to provide a thicker film. The resulting film was 290 ± 10 nm thick as measured by the AFM. The substrate and film was then baked at 140 °C for at least 30 min in a vacuum oven at ~500 mbar pressure.

Following exposure the film was developed in pure methyl isobutyl ketone for 60 s at 25 ± 0.5 °C, during which time the developer was agitated mildly. Following development, the sample was immediately rinsed in isopropyl alcohol for 5 s, dried with a jet of clean freon, and baked again at 140 °C for 30 min.

B. System setup

Figure 1 shows the experimental arrangement. Broadband incoherent VUV light was generated using a laser-produced plasma. Pulses from a Q-switched Nd:YAG laser were fo-

[a]Present address: Department of Optics and Quantum Electronics, JATE University, H-6720 Szeged, Dóm tér 9, Hungary.
[b]Permanent address: Research Institute for Solid State Physics, P.O. Box 49, H–1525, Budapest, Hungary.
[c]Electronic mail: young@rice.edu

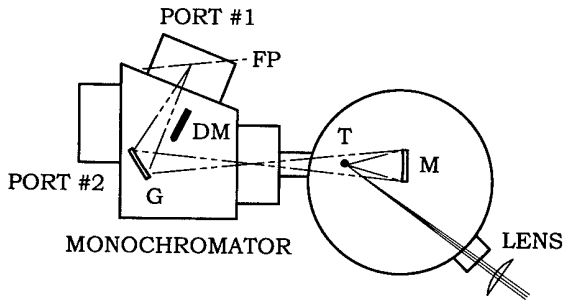

FIG. 1. Experimental arrangement for the resist characterization. The incoming Nd:YAG laser pulse (solid lines) was focused to the target rod **T**, and the VUV radiation (dash-dot-dot lines) was collected and imaged by the gold mirror **M**. The grating **G** filtered and focused the VUV light to the focal plane **FP**, which was tangential to the Rowland circle. The energy could be monitored during the exposure by turning the diverter mirror **DM** into and out from the beam path.

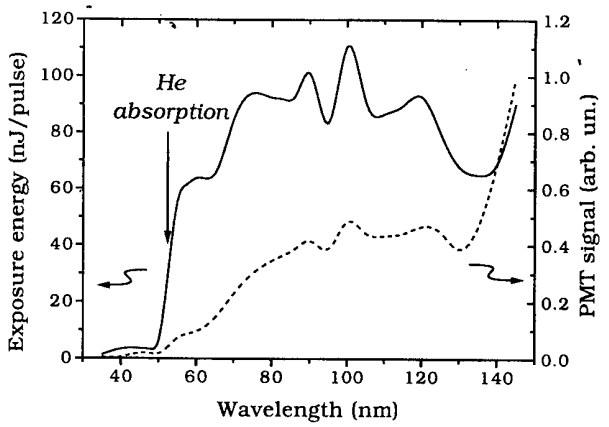

FIG. 3. Typical spectrum of the laser produced plasma light source used in the experiments, as measured directly by the PMT at Port No. 2 (dashed line), and the calibrated light energy deposited on the sample surface at Port No. 1 (solid line).

cused onto a 6 mm diameter stainless steel rod with a 30 cm focal length lens. The 930± 10 mJ and 7 ns full width at half maximum (FWHM) pulses produced infrared light intensity of 10^{12} W cm^{-2} at the target surface. The target rod was attached to and rotated by the motorized screw[14] to present a fresh target surface for each laser pulse. The laser repetition rate was 10 Hz and this arrangement allowed 75 min long exposures. The light from the laser-produced plasma was collected by a 2 in. diameter spherical gold mirror (focal length of 5 cm) and imaged on the input slit of a 0.2 m, *f* #4.5 monochromator. High purity helium at 20 Torr was flowed through the chamber during the exposures to reduce the accumulation of plasma debris on the mirror.

For the PMMA exposures, the monochromator was modified by replacing the output slit at Port No. 1 with a sample holder tangent to the Rowland circle, allowing us to make exposures at several wavelengths simultaneously. The monochromator grating had 1200 lines/mm leading to a plate factor of 3.4 nm/mm in the focal plane. Exposures were made through a mask (see Fig. 2) with identical patterns spaced 1.25 mm apart, corresponding to 4.25 nm in wavelength. The five patterns spanned a total wavelength region of 17 nm. The input slit was set at 1.25 mm for all exposures. The mask was fabricated from 75 μm thick polyimide sheet by ablation using a KrF excimer laser. As seen in Fig. 2, each of the five mask patterns consist of two bars, 60 μm wide by 2.5 mm long, separated by a 20 μm diameter circle. Film depth measurements were made on the circular dot exposures; the bars served only as visual aids to locate the circles. The mask was placed directly against the PMMA film and the assembly held in the monochromator's focal plane.

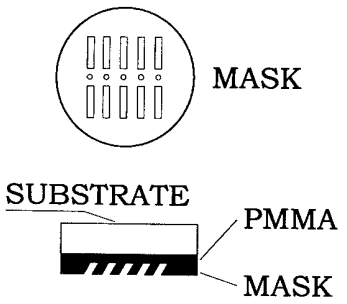

FIG. 2. Front view of the polyimide mask and cross section of the substrate, film, and mask assembly.

C. Calibration of VUV exposure flux

The determination of the depth versus exposure characteristics of PMMA requires careful measurement of the exposure flux over a range of wavelengths. Our primary energy standard was the well studied and stable quantum efficiency of Al_2O_3 cathode photodiodes.[15] Because the sensitivity of this photocathode drops sharply for wavelength longer than 100 nm, we used it primarily to calibrate a sodium salicylate-photomultiplier combination (PMT) that was used to measure the source spectrum and to monitor exposure values. The variation of the quantum efficiency of sodium salicylate is about 5% over our 35–130 nm wavelength measurement range.[15]

As a first step of calibration, we measured the energy at monochromator Port No. 1 with the Al_2O_3 photodiode in the 60–100 nm wavelength range. During the calibration the input and output slits were opened to 100 μm. The spectrum was then recorded by the PMT at the same port and calibrated by the results from the Al_2O_3-photodiode measurement. Next, the spectrum was recorded at Port No. 2 and the reflection of the diverter mirror was calibrated by comparing the two spectra. Using this method we were able to evaluate the energy at Port No. 1 from the measured signals of the PMT at Port No. 2 at each wavelength between 50 and 130 nm (Fig. 3). The exposure energies varied between 60 and 120 nJ per laser pulse. We estimate that the error of the absolute energy values is 20%, while the relative error between different wavelengths is only 12%. The energy density at the sample plane was between 7.0×10^{-4} and 1.4×10^{-3} mJ cm^{-2} per pulse, as calculated by dividing the measured energy by the effective open area of the output slit. The total

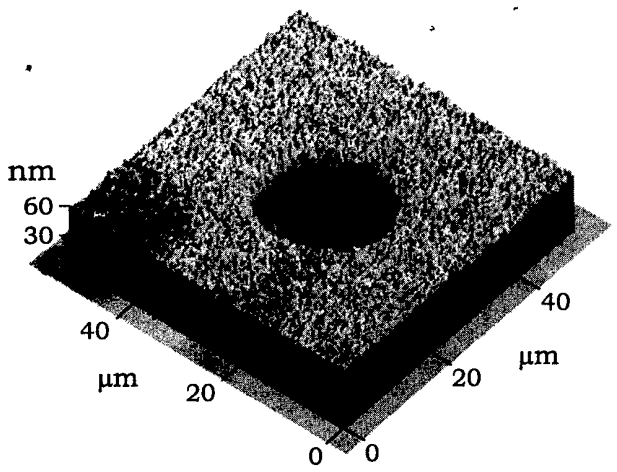

FIG. 4. An atomic force micrograph of a contact printed pattern on the surface of PMMA.

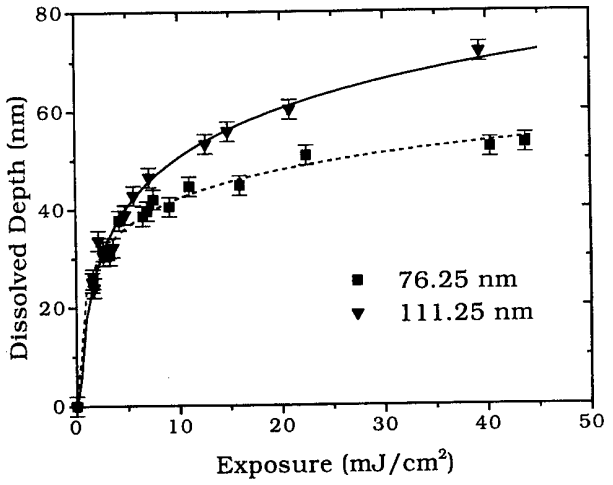

FIG. 5. Developed film depth vs exposure for PMMA at two different wavelengths. The symbols with error bars are the measured height differences between exposed and unexposed regions, while the lines are the results of a model fitted to the data.

exposure was obtained by simply multiplying this average exposure value per laser pulse by the total number of pulses in an exposure.

In order to account for possible long-term changes in the efficiency of the laser-produced plasma and the light collection system, we interrupted each exposure to take source spectra at Port No. 2. The number of spectra taken was varied to achieve good average values. Three spectra were measured for the shortest (3 and 4 min) exposures and seven for the longest (60 min) exposures. The exposure energy was calculated by averaging the spectra.

D. Depth measurement by AFM

The transverse and vertical scans of the AFM[16] were calibrated using a calibration grating and height standards. A typical atomic force micrograph of a contact printed test pattern on the surface of the PMMA is shown in Fig. 4. To obtain a good estimate of the depth of a given hole, four $\sim 50 \times 50$ μm (256 by 256 pixels) scans were made using different scanning directions and the results averaged. Typically, the standard deviation of the pixel height from the average was ~ 3 nm. However, because of the large number of pixels, this deviation did not effect the depth measurement directly, since the *average* height of the pixels were compared. However, this high frequency noise did introduce errors during the removal of the apparent surface curvature. Apparent surface curvature is an inherent byproduct of the AFM transverse scanning mechanism, and it can be well approximated by a second order polynomial. The elimination of the curvature was performed by fitting a second order polynomial to each data row of the scans. The accuracy of this fit is reduced by the pixel height variation because of the small number of pixels in each row. This was particularly true where the data row contained values from both the exposed and unexposed parts, since the unexposed part was not included in the fitting. We estimate that the vertical resolution was limited to 2 nm by this effect.

III. RESULTS AND DISCUSSION

Measurement of exposure patterns such as Fig. 4 resulted in characteristic curves of depth versus exposure, S, at specific wavelengths spaced 4.25 nm over the range of 59–128 nm. Figure 5 shows two such curves; the symbols represent measured data while the lines are the result of the exposure-dissolution model discussed below. This set of curves can be usefully summarized by defining a specific exposure flux, S_p, for each wavelength that will produce a 30 nm deep pattern. Figure 6 shows a plot of S_p over the wavelength range measured. While the 30 nm criteria is arbitrary, we found that patterns of this depth resulted in low noise, reproducible measurements. Also shown in Fig. 6 is the calculated derivative of pattern depth versus exposure, $G = dz/dS$, evaluated at S_p. The parameter G is a measure of the exposure resolution; a large G indicates there are more distinguishable intensity levels within a given exposure range.

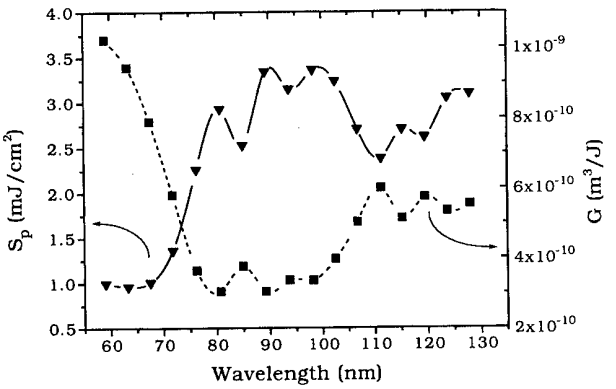

FIG. 6. Specific exposure S_p required for a developed depth of 30 nm, (triangles), as a function of wavelength, and G, the derivative of depth with respect to exposure at S_p (filled squares), characterizing the possible grey-scale levels for imaging applications.

TABLE I. Values of α and κ determined by fitting the model of Eq. (3) to the measured dissolved pattern depth. The wavelength independent value of $n=2.43$.

λ_c (nm)	α (μm^{-1})	κ ($m^{2n+1}/J^n s$)
59.00	98	5.3×10^{-10}
63.25	110	1.3×10^{-9}
67.50	126	3.5×10^{-9}
71.75	126	1.7×10^{-9}
76.25	121	3.6×10^{-10}
80.75	112	9.8×10^{-11}
85.00	105	8.8×10^{-11}
89.25	98	2.8×10^{-11}
93.75	94	2.5×10^{-11}
98.25	88	1.5×10^{-11}
102.50	78	7.8×10^{-12}
106.75	73	9.2×10^{-12}
111.25	70	1.0×10^{-11}
115.25	72	8.4×10^{-12}
119.50	66	6.3×10^{-12}
123.75	61	3.1×10^{-12}
128.00	57	2.4×10^{-12}

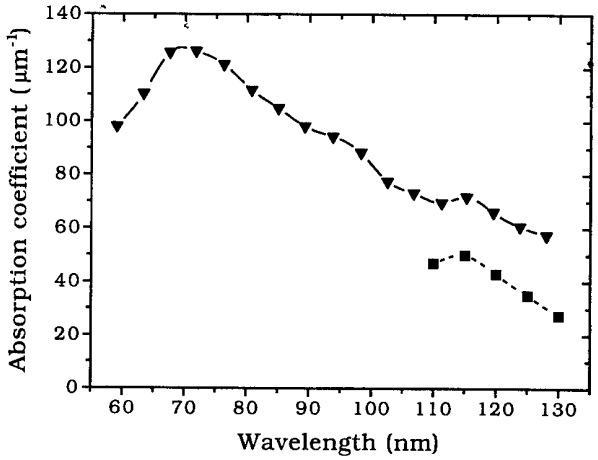

FIG. 7. Absorption coefficient of PMMA as a function of the wavelength (triangles) calculated by fitting the measured pattern depths to the model of Eq. (3). The data shown by filled squares were determined by Kudo *et al.*, by direct absorption measurement (Refs. 10 and 11).

A. Dissolution model of PMMA

We used a simple model of exposure energy deposition and the resulting dissolution of PMMA to calculate the VUV absorption coefficient of PMMA from our pattern depth data. First, we assumed a simple exponential absorption in PMMA so that the energy deposited at any depth z is $D(z)=\alpha S\exp(-\alpha z)$, where α is the absorption coefficient, and S is the incident energy flux at the surface $z=0$. Next, we used the previously proposed model of polymer dissolution[2,3] that postulates the dissolution rate is proportional to a power of the energy deposited per unit volume:

$$\frac{dz}{dt}=[kD(z)]^n+R_0, \tag{1}$$

where n is a constant and R_0 is the dissolution rate of the unexposed polymer. The parameter k represents the bond breaking efficiency of the radiation and is expected to be a function of wavelength.[3] Substituting for $D(z)$, the change of surface height with development time is

$$\frac{dz}{dt}=\kappa S^n e^{-\alpha z(t)n}+R_0, \tag{2}$$

where $\kappa=\alpha^n k^n$. Assuming $z(0)=0$ and $t=0$ at the start of the development, the solution of Eq. (2) is

$$z(t)=\frac{1}{n\alpha}\ln\frac{R_0 e^{\alpha R_0 t n}+(e^{\alpha R_0 t n}-1)\kappa S^n}{R_0}. \tag{3}$$

This model neglects temperature dependence of the dissolution rate and any dependence of the exponent n on deposited energy.[2,17]

B. Resist characteristics

We evaluated R_0 by immersing unexposed PMMA samples in methyl isobutyl ketone for various times and measuring the change in thickness with the AFM. We found that $R_0=72.3\pm18$ pm s^{-1}, which agrees well with the value of 80 pm s^{-1} of Hawryluk *et al.*[2] Equation (3) was fitted to the experimental data in order to determine the parameters $\alpha(\lambda)$, $\kappa(\lambda)$, and n. The exponent n should depend only on the polymer and solvent properties and it was assumed to be independent of wavelength in the fitting process. Therefore, a simultaneous fitting has been performed for the data from the 17 different wavelengths in order to find the best $(17\times2)+1$ parameters (α and κ for each λ, and one common n) for all the experimental data. Using this method of simultaneous fitting of all the wavelength data — instead of a series of independent three-parameter fittings for each λ — we were able to fit our developed depth versus exposure and wavelength data very well; two examples are shown in Fig. 5. Since the data values in Fig. 5 represent the difference in height of exposed and unexposed areas, the curves plotted are $z(t)$ from Eq. (3) minus $R_0 t$, the amount dissolved from the unexposed regions. For our conditions the correction $R_0 t=4.3$ nm. Values of $\alpha(\lambda)$ and $\kappa(\lambda)$ are given in Table I for each wavelength measured, and the absorption coefficient is plotted in Fig. 7. The 95% confidence interval of the fitted parameters have also been determined: they are $\pm4\%$, $\pm11\%$, and $\pm31\%$, for the values of n, α, and κ, respectively. The optimum value of n was found to be 2.43. Previous studies using x-ray exposure found values between 3 and 3.4, while electron beam exposure yielded values of 1.33 to 2.58.[2] The calculated absorption coefficient in Fig. 7 is systematically higher than the values measured by Kudo *et al.*,[10,11] in the range 110–130 nm. This discrepancy might indicate the need for a more comprehensive dissolution model, e.g., incorporation of the D dependence of n.

IV. SUMMARY AND CONCLUSIONS

We have presented the depth versus exposure characteristics of PMMA over a broad VUV spectral region, 59–128 nm. These curves provide essential information for image

reconstruction of contact and holographic recordings. We found that exposures as small as 2 $mJ\,cm^{-2}$ can produce patterns 20 nm deep. Since the AFM can resolve ~2 nm depth differences, about ten vertical or exposure levels are distinguishable. This exposure level is significantly lower than that previously used with other depth measurement techniques.[1,5] Further improvement should be possible by decreasing the pixel noise, perhaps by modifying the film preparation and developing procedures.

ACKNOWLEDGMENTS

This work was jointly supported by the National Science Foundation, and the U.S. Air Force Office of Scientific Research.

[1]G. D. Kubiak *et al.*, in *OSA Proceedings on Soft-X-Ray Lithography*, edited by J. Bokor (Optical Society of America, Washington, DC, 1991), Vol. 12, pp. 124–128.
[2]R. J. Hawryluk, H. I. Smith, A. Soares, and A. M. Hawryluk, J. Appl. Phys. **46**, 2528 (1975).
[3]J. S. Greeneich, J. Electrochem. Soc. Solid State Sci. Technol. **122**, 970 (1975).
[4]*X-Ray Microscopy III*, edited by A. G. Michette, G. R. Morrison, and C. J. Buckley (Springer, Berlin, 1992).
[5]G. C. Bjorklund, S. E. Harris, and J. F. Young, Appl. Phys. Lett. **25**, 451 (1974).
[6]M. Howells *et al.*, Science **238**, 514 (1987).
[7]K. Shinohara, A. Ito, and Y. Kinjo, in *Applications of Laser Plasma Radiation* (SPIE, Bellingham, WA, 1994), Vol. 2015, pp. 10–19.
[8]R. A. Cotton *et al.*, in *Applications of Laser Plasma Radiation* (SPIE, Bellingham, WA, 1994), Vol. 2015, pp. 86–96.
[9]A. D. Stead, A. M. Page, and T. W. Ford, in *Applications of Laser Plasma Radiation II* (SPIE, Bellingham, WA, 1995), Vol. 2523, pp. 40–50.
[10]K. Kudo *et al.*, Jpn. J. Appl. Phys. 1 **29**, 2572 (1990).
[11]K. Kudo *et al.*, Jpn. J. Appl. Phys. 1 **31**, 401 (1992).
[12]J. C. White *et al.*, Appl. Phys. Lett. **44**, 22 (1984).
[13]PMMA 950k Resist in Chlorobenzene, Cat. No. 897631, OCG Microelectronics, 3 Garret Mauntain Plaza, West Paterson, NJ 07424.
[14]Picomotor, New Focus, Inc., 2630 Walsh Avenue, Santa Clara, CA 95051.
[15]J. A. Samson, *Techniques of Vacuum Ultraviolet Spectroscopy*, 2nd ed. (Pied, Lincoln, NE, 1980).
[16]AutoProbe Microscope System, Park Scientific Instruments, 1171 Borregas Ave., Sunnyvale, CA 94089.
[17]G. H. Bernstein, D. A. Hill, and W. Liu, J. Appl. Phys. **71**, 4066 (1992).

Comparison of Laser-Produced Plasma Target Materials for Pumping the 109-nm Xe^{2+} Auger Laser

Tasshi Dennis, Hendrik Matthew Duiker, Jun Wu, Csaba Tóth, and James F. Young, *Senior Member, IEEE*

Abstract— **We compared cadmium, copper, gold, and zinc targets to stainless steel for laser-produced plasma pumping the Xe^{2+} 109 nm laser. A unique target geometry allowed us to measure the laser output using two materials under identical conditions. Small signal gain coefficients and maximum output powers are presented for each material relative to stainless steel; we observed a ~20% improvement in the gain coefficient and a ~112% improvement in total energy using a cadmium target. This increase probably results from an improved overlap of the laser-produced plasma emission spectrum with the Xe inner shell 4*d* photoionization cross section, although published data to support this hypothesis are scarce and inconsistent.**

I. Introduction

LASER-PRODUCED plasmas have proven to be convenient pumping sources for vacuum ultraviolet (VUV) lasers [1]–[6]. In these experiments, a short pulse length laser is focused to high intensity on a metal target, forming and heating a high density, highly ionized plasma. Typically, the focal region is a line with a power density of 10^{11}–10^{13} W cm^{-2}. The hot plasma radiates incoherent soft x-rays into the surrounding gas, and creates a population inversion either through direct photoionization or via collisions with energetic electrons produced by photoionization. The practicality of this pumping method, and of the VUV lasers, depends critically on the conversion efficiency of laser light into soft x-ray radiation with the required spectrum, since higher efficiency reduces the size and cost of the pumping laser system. VUV lasers are single-pass amplifiers seeded by spontaneous emission, with much of the gain length operating in the small-signal exponential gain regime; thus, small improvements in pumping efficiency can yield large improvements in output power and overall efficiency.

The 109-nm Xe^{2+} Auger laser is a promising practical source of VUV radiation because of its unique combination of high gain, efficiency, benign physical properties, and short wavelength. It is pumped by photoionization of an inner shell 4*d* electron, followed by rapid, selective Auger decay to the upper laser level. The threshold for Xe 4*d* photoionization is 68 eV, with a peak cross section of 3×10^{-17} cm^2 at 100 eV, and a full width at half maximum of about 40 eV [7]. In this range, the photoionization cross section for 4*d* inner electrons is about ten times larger than that for the outer 5*s*, 5*p* electrons.

Several target materials have been used previously for the Xe^{2+} laser. The first observations of gain in the Xe Auger system were reported in 1986 using a tantalum target [2]. G. Yin *et al.* also used tantalum in their optimization studies [8]. In 1987, Sher *et al.* used an electroplated gold target and a new pump geometry, and reported the first saturated Xe^{2+} laser output [9]. In later experiments, this group also reported results using a stainless steel target [10]. Our initial Xe^{2+} laser system also used a stainless steel target, primarily because of its simplicity [11]. Since the pump laser energy, pulse length, and focused intensity on target vary considerably among these experiments, it is difficult to isolate the effect of the target material on Xe^{2+} laser performance. Recently, however, the performance of a self-healing Hg-coated gold target has been compared to that of a plain gold target under comparable conditions; the two had similar performance [12].

We present the first experiments that quantitatively compare cadmium, copper, gold, zinc, and stainless steel plasma targets for pumping the 109-nm Xe^{2+} Auger laser under identical experimental conditions. Use of a cadmium target more than doubles the laser output energy for a 112% improvement. This increase probably results from an improved overlap of the laser-produced plasma emission spectrum and the Xe inner shell 4*d* photoionization cross section.

II. Experiment

The general pumping configuration has been described previously [11]. In summary, a Coherent Antares 76-s Nd:YAG CW mode-locked oscillator provides a 76 MHz train of ~100 ps or ~200 ps [13] long pulses at 1064 nm. A Continuum RGA-69 pulsed regenerative amplifier and an additional amplifier are used to amplify selected pulses to an energy of about 260 mJ. Relay imaging optics [14] are used throughout to maintain fringe-free beam patterns; the system operates at 6 Hz. As shown in Fig. 1, the pump beam is focused to a ~75 μm-wide by 20-cm-long line on the grooved target using a cylindrical mirror at an 83° angle of incidence, resulting in a power density of about 10^{11} W cm^{-2}.

The basic plasma target is a machined stainless steel rod 3.8 cm in diameter and 20-cm long, threaded at ~30 grooves per centimeter. The sample material was electroplated over half the circumference of the basic target, while the other half

Manuscript received April 29, 1995; revised July 5, 1995. This work was supported by the US Air Force Office of Scientific Research and the National Science Foundation.

T. Dennis, H. M. Duiker, J. Wu, and J. F. Young are with the Department of Electrical and Computer Engineering, and the Rice Quantum Institute, Rice University, P.O. Box 1892, Houston, TX 77251 USA.

Cs. Tóth is with the Research Institute for Solid State Physics, P.O. Box 49, H-1525, Budapest, Hungary.

IEEE Log Number 9414557.

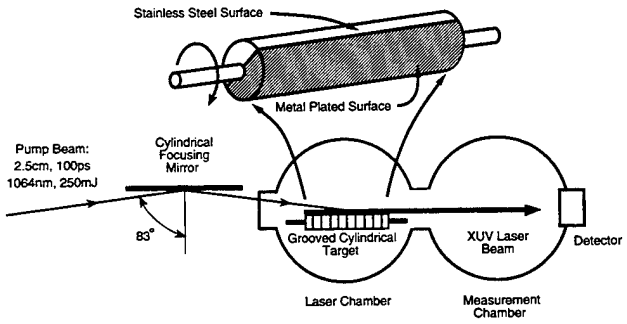

Fig. 1. Target geometry for the 109-nm Xe^{2+} Auger laser.

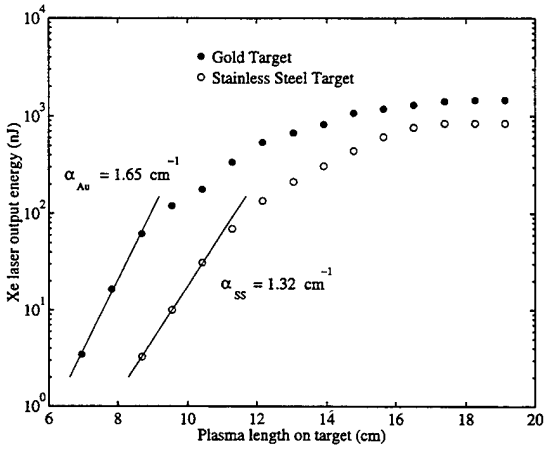

Fig. 2. Xe laser output energy versus plasma length for the gold-stainless steel target.

was left unplated to provide a reference signal from stainless steel. Targets were prepared using cadmium, copper, gold, and zinc. The plating company estimated the thickness to be 12 μm for the gold, and about 75 μm for the others. Rotation of the rod during laser operation exposed alternating sections of stainless steel and the plated sample material to the pump pulses.

The target rod is housed in a vacuum cell containing ~15 Torr of Xe gas. The output intensity of the forward propagating 109-nm beam was measured with an aluminum oxide cathode photodiode and oscilloscope. The length of the target pumped was varied using a moveable knife edge placed in the pump beam outside the target chamber. For each pumped length, the laser output energy was recorded for both the stainless steel and the plated metal regions as the target rotated. In this manner, data for the sample material and stainless steel were collected in alternating measurements while maintaining near-identical pumping conditions.

III. Results

Fig. 2 shows a semi-logarithmic plot of the data obtained using a stainless steel target with a gold plated region. Measurable output energy was obtained for a pumped length of only ~7 cm from the gold target region, whereas the stainless steel region required nearly 9 cm. The first three points of each curve were fit to a straight line to estimate the small signal gain coefficients: approximately 1.6 cm^{-1} for gold, and 1.3 cm^{-1} for stainless steel. For both materials, the

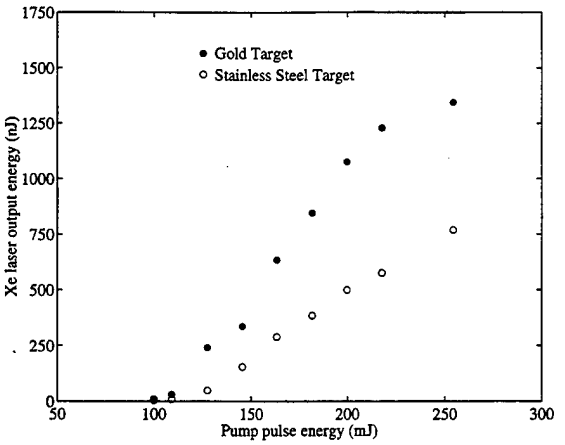

Fig. 3. Xe laser output energy versus pump energy for the gold-stainless steel target.

TABLE I
Performance of Target Materials Relative to Stainless Steel

Material	Total output improvement	Small signal gain improvement
Cadmium	112%	20%
Zinc	100%	11%
Gold	100%	25%
Copper	25%	-

output energy dependence on pumped length deviated strongly from exponential for target lengths greater than 13 cm. We also investigated the pump energy dependence for full target illumination. Fig. 3 shows that the gold target produced about twice the Xe^{2+} laser output energy as the stainless steel target over the full range of pump energies. This data, and that for the other target materials, are summarized in Table I. Plots for the gold-stainless steel target have been presented as a comparison reference to previous Xe^{2+} laser studies.

Standard deviations of less than ±10% were easily acheivable for each data point. The error range was largely dependent on the pump laser noise. We also observed minor variations between the different stainless steel targets. We attribute this variation to minor changes in pump-beam focusing, in Xe pressure, and/or in the characteristics of the pump-laser system during the period required to change targets. Furthermore, systematic changes in output over longer periods of time were the result of modifications and improvements in the pump-laser system. For example, pump-pulse durations of 200 ps were used for the gold-stainless steel target, while shorter, more powerful 100-ps pulses were subsequently used for all other targets. Thus, near-simultaneous comparison of sample materials to a standard surface is essential to get consistent results.

Consistency of output and target lifetime are also important criteria in selecting a target material. We have noticed that for new stainless-steel targets, the first few pump pulses at a fixed

location produce less 109-nm output energy than subsequent pulses. Apparently, the initial pulses remove oxides or other residue that reduce plasma production efficiency, and we routinely expose a new target to a series of pump pulses before beginning measurements to insure consistency. We observed the same behavior for both cadmium and zinc; several initial pump pulses at a fixed position were necessary to prepare the surface, while the next thirty or more shots in the same location showed little signal fluctuation. The gold-plated target surface did not appear to require any initial "cleaning." In contrast, the copper plated target exhibited large pulse-to-pulse fluctuations in laser output; so large, in fact, that we were unable to make reliable measurements of the small signal gain coefficient.

Surface ablation obviously limits the lifetime of plated targets; when the gold-plated target was held stationary so that the pump repeatedly illuminated the same region, the 109-nm output signal was constant for about the first twenty pump pulses, after which the signal decreased to the stainless-steel value as the plating was ablated. The thicker zinc and cadmium surfaces lasted more than twice as long. Our target circumference consists of 1600 75-μm-wide strips, so a cadmium-plated target should have a lifetime greater than 6.4×10^4 pulses, or about three hours at our pulse rate. Bulk, machined zinc- or cadmium-target rods are probably possible (most research budgets cannot accommodate solid-gold target rods), but even solid targets have a finite lifetime. Ablation removes the groove edges, and the rods must be remachined, perhaps after every 50 hours of use for stainless steel. Target ablation also produces debris that ultimately deposits on chamber surfaces. The cadmium, gold, and zinc targets seemed to produce about equal amounts of debris, all somewhat more than from a stainless steel target. The copper target rapidly produced heavy debris contamination of the laser chamber. The mercury-wetted target of Yamakoshi *et al.* [12], represents a clever method for avoiding ablation and debris problems while providing a high-atomic number target surface.

IV. Discussion

We have observed a ~20% improvement in the gain coefficient and a ~112% improvement in total energy for a Xe^{2+} 109-nm laser by plating the stainless-steel target with cadmium. Significant improvements in output using zinc and gold were also observed. Use of these targets for the Xe^{2+} laser can reduce the required pump energy or reduce exposure times for applications such as imaging or photochemistry. With a copper target, the 109-nm laser output exhibited large pulse-to-pulse fluctuations, with the best values only slightly larger than those for the stainless steel target. The fluctuations appeared to result from the presence of surface oxides and a more rapid copper surface ablation. The rapid generation of copper debris, coupled with only a minor improvement in output energy, make copper targets a poor choice for the Xe^{2+} 109-nm laser.

It is reasonable to attribute the significant improvement in 109-nm laser output energy using a cadmium target to a higher pump to soft x-ray conversion efficiency and/or to improved spectral properties. There are two plasma spectral factors that could be important. Increased plasma emission at 100 eV, overlapping the Xe inner shell $4d$ photoionization cross section, would enhance the production of the upper laser level; in contrast, increased output of low energy photons could reduce gain by ionizing the upper laser level to Xe^{3+} (requiring about 7 eV), or by ionizing neutral Xe (12.1 eV) and producing extra electrons, which are believed to quench the Xe^{2+} gain [2]. Although several authors report spectra of laser-produced plasmas for different target materials, the experimental conditions were generally quite different from those used for the Xe^{2+} laser, and low photon energy spectra were not measured.

Table II summarizes the experimental conditions of the more relevant spectral studies and highlights their differences compared to our study. Mochizuki *et al.* [15] focused 532-nm, 1-ns-long pulses to a density of 10^{14} W cm^{-2}, nearly 1000 times higher than the density used here, onto a large number of target materials. Fig. 13(a) in that paper shows that the conversion efficiency into the 100–200 eV band, the lowest energies measured, varies only moderately with atomic number for elements heavier than copper; certainly the efficiency of copper and gold appear identical under these conditions. Chaker *et al.* [16], present experimental and theoretical conversion efficiencies as a function of atomic number using a 1064-nm, 500-ps-long pump pulse focused to a density of 4×10^{13} W cm^{-2}. Their theoretical curve for conversion into the 100–750 eV band shows a periodic dependence with variations of about a factor of three. Their measurements of copper and gold targets match the theory, with gold yielding 2.5 times the efficiency of copper. They did not measure a cadmium target, but it would fall at a minimum of their calculated curve, with an efficiency about equal to copper, in contrast to our results. Gerritsen *et al.* [17] present experimental data from fifteen target materials using a 532-nm 15-ns-long pump, focused to 7×10^{12} W cm^{-2}. The conversion efficiency into the 250–800 eV band shows peaks corresponding to atomic shells. The peaks, however, are shifted from the theory of Chaker *et al.* with maxima near titanium (atomic number $Z = 22$), cadmium ($Z = 48$), and gold ($Z = 79$). The yield for gold was also about twice that of copper, while the maximum at cadmium was about 25% above that of gold. This is more consistent with our observations, except this data also indicates that an iron or nickel target (the main components of stainless steel) would have a yield slightly better than a copper target.

Perhaps more relevant are the detailed emission spectra (resolution ~7 eV) from 100–330 eV, shown in Fig. 6(a) of Gerritsen *et al.* Iron and copper show about equal yields at 100 eV, while gold is 30% higher. Cadmium was not measured, but it is spanned in atomic number by silver ($Z = 47$), having a yield 40% higher than iron, and by tin ($Z = 50$) with a yield about equal to iron. From these curves, the best target materials for the Xe^{2+} laser appear to be tantalum ($Z = 73$) and lead ($Z = 82$), both with yields at 100 eV over twice as high as iron and 50% greater than gold. Tantalum is very difficult to machine and to electroplate. We tried several stainless-steel target rods that were "flame-sprayed" or plasma deposited with tantalum [18]. These coatings are very granular; thick coatings filled in the grooves and thin coatings were irregular. We were unable to observe any 109-nm output using these targets. While the efficiency of a lead-plated target might be high, we

TABLE II
SUMMARY OF LASER PRODUCED PLASMA SPECTRAL STUDIES

Reference	Figure number	Intensity [Wcm^{-2}]	Pump wavelength [nm]	Pump pulse length [nsec]	Photon energy range [eV]
Mochizuki, et al. [15]	13(a)	$\sim 1 \times 10^{14}$	532	1	100–200
Chaker, et al. [16]	7(a)	$\sim 4 \times 10^{13}$	1064	0.5	100–750
Gerritsen, et al. [17]	8	$\sim 7 \times 10^{12}$	1064	15	250–800
Gerritsen, et al. [17]	6(a)	$\sim 7 \times 10^{12}$	1064	15	100–330
Kauffman, et al. [19]	3	$\sim 10^{11}$	532	7.5	92–100
Spitzer, et al. [20]	3, 4	$\sim 1 \times 10^{11}$	532	7.5	50-250, 80-150
Yamakoshi, et al. [12]	3	$\sim 3.5 \times 10^{10}$	1064	0.4	Xe^{2+} laser
This work	–	$\sim 10^{11}$	1064	0.1–0.2	Xe^{2+} laser

suspect that the output consistency and debris problems would be very similiar to those of copper.

The most pertinent work in terms of experimental conditions would appear to be that of Kauffman *et al.* [19]. They performed a Z-scaling study for sixteen materials, recording x-ray conversion efficiency into a narrow ~8-eV band centered at 96.5 eV. While the pump excitation wavelength was shorter (532 nm) and the pulse duration was longer (7.5 ns) than in our studies, the intensity on target was comparable at $\sim 10^{11}$ W cm^{-2}. Their results also show peaks corresponding to atomic shells, but shifted from those of Chaker *et al.* and Gerritsen *et al.* The yield for gold was nearly twice that of copper, and the cadmium yield fell between copper and gold. Again, iron and nickel targets had a yield equal to or better than copper. The results of Gerritsen *et al.* and Kauffman *et al.* are very similar, despite recording different energy ranges. Thus, even under the most similar experimental conditions, their measurements do not fully explain our observations, perhaps indicating the importance of the low photon energy spectra of different targets.

The studies cited above, as well as our own work, indicate that target materials of high atomic number are likely to be more efficient for pumping the Xe laser. Yet, it is simplistic to think that target atomic number is the only important parameter, or even an independent parameter. This is shown clearly in the work of Spitzer *et al.* [20], who made detailed spectral measurements of laser-produced plasma efficiency in the range of 50–250 eV for gold and tin targets. Both gold and tin have (at least local) emission peaks near 100 eV that match the Xe inner shell photoionization, so it is not surprising that we found gold to be a good target material. However, the pump conversion efficiency into the 80–150-eV band varies significantly with focal spot size and power density, and *the dependence is different for the two materials.* For example, the conversion efficiency for tin maximizes at a value of focal power density which depends on spot size. In contrast, the efficiency of a gold target shows no maximum in the range studied, but increases steadily with power density for all spot sizes. Similarly, Yamakoshi *et al.* [12] found that the Xe^{2+} gain coefficient using a mercury target was higher than that for gold at a pump power intensity of 1×10^{10} W cm^{-2}, while the situation was reversed at 3.5×10^{10} W cm^{-2}.

Our work has shown that a simple change of target material can result in significant improvements in the Xe^{2+} 109-nm laser performance. At the same time, it is clear that we have explored only part of the full parameter space of target conditions, and our ranking of materials would probably change for different conditions of pump wavelength, pulse length, power density, and focal geometry. Our results represent a good starting point for a detailed optimization of pumping conditions in other situations.

REFERENCES

[1] H. C. Kapteyn and R. W. Falcone, "Auger-pumped short-wavelength lasers in xenon and krypton," *Phys. Rev. A,* vol. 37, pp. 2033–2038, 1988.

[2] ——, "Observation of a short-wavelength laser pumped by Auger decay," *Phys. Rev. Lett.,* vol. 57, pp. 2939–2942, 1986.

[3] S. J. Benerofe, G. Y. Yin, C. P. J. Barty, J. F. Young, and S. E. Harris, "116 nm H_2 laser pumped by a traveling-wave photoionization electron source," *Phys. Rev. Lett.,* vol. 66, pp. 3136–3139, 1991.

[4] D. J. Walker, C. P. J. Barty, G. Y. Yin, J. F. Young, and S. E. Harris, "Observation of super Coster–Kronig pumped gain in Zn III," *Opt. Lett.,* vol. 12, pp. 894–896, 1987.

[5] C. P. J. Barty, G. Y. Yin, J. E. Field, D. A. King, K. H. Hahn, J. F. Young, and S. E. Harris, "Studies of a 96.9 nm laser in neutral cesium," *Phys. Rev. A,* vol. 46, pp. 4286–4296, 1992.

[6] C. Tóth, J. F. Young, and R. Sauerbrey, "Optical gain in the ionic excimer $Cs^{2+}F^-$ excited by soft x-rays from a laser-produced plasma," *Opt. Lett.,* vol. 18, pp. 2120–2122, 1993.

[7] D. M. P. Holland, K. Codling, J. B. West, and G. V. Marr, "Multiple photoionisation in the rare gases from threshold to 280 eV," *J. Phys. B: Atomic Molecular Phys.,* vol. 12, no. 15, pp. 2465–2484, 1979.

[8] G. Y. Yin, C. P. J. Barty, D. A. King, D. J. Walker, S. E. Harris, and J. F. Young, "Low-energy pumping of a 108.9 nm xenon Auger laser," *Opt. Lett.,* vol. 12, pp. 331–333, 1987.

[9] M. H. Sher, J. J. Macklin, J. F. Young, and S. E. Harris, "Saturation of the Xe III 109 nm laser using traveling-wave laser-produced-plasma excitation," *Opt. Lett.,* vol. 12, pp. 891–893, 1987.

[10] M. H. Sher, S. J. Benerofe, J. F. Young, and S. E. Harris, "2-Hz 109 nm mirrorless laser," *J. Opt. Soc. Amer. B,* vol. 8, pp. 114–116, 1991.
[11] T. S. Clement, C. Tóth, J. Wu, and J. F. Young, "A reasonably practical XUV laser for applications," *IEEE J. Quantum Electron.,* vol. 30, pp. 2136–2140, 1994.
[12] H. Yamakoshi, C. T. Chin, S. Jaimungal, P. R. Herman, F. Budnik, G. Kulesár, L. Zhao, and R. S. Majoribanks, "Extreme-ultraviolet laser photo-pumped by a self-healing Hg target," *Applicat. Laser Plasma Radiation,* vol. 2015, Bellingham, WA 98227-0010, SPIE, 1993.
[13] C. Tóth, "Simple optical pulse lengthening setup for the subnanosecond range," *Opt. Photon. News/Eng. Lab. Notes,* vol. 6, no. 8, Aug. 1995.
[14] J. T. Hunt, J. A. Glaze, W. W. Simmons, and P. A. Renard, "Suppression of self-focusing through low-pass spatial filtering and relay imaging," *Appl. Opt.,* vol. 17, no. 13, pp. 2053–2057, 1978.
[15] T. Mochizuki, T. Yabe, K. Okada, M. Hamada, N. Ikeda, S. Kiyokawa, and C. Yamanaka, "Atomic-number dependence of soft x-ray emission from various targets irradiated by a 0.53 μm wavelength laser," *Phys. Rev. A,* vol. 33, pp. 525–539, 1986.
[16] M. Chaker, H. Pépin, V. Bareau, and B. Lafontaine, "Laser plasma x-ray sources for microlithography," *J. Appl. Phys.,* vol. 63, pp. 892–899, 1988.
[17] H. C. Gerritsen, H. van Brug, F. Bijkerk, and M. J. van der Wiel, "Laser-generated plasma as soft x-ray source," *J. Appl. Phys.,* vol. 59, pp. 2337–2344, 1986.
[18] Flame Spray Coating Co., Inc., 33847 Doreka, Fraser, MI 48026.
[19] R. L. Kauffman, D. W. Phillion, and R. C. Spitzer, "X-ray production ~13 nm from laser-produced plasmas for projection x-ray lithography applications," *Appl. Opt.,* vol. 32, no. 34, pp. 6897–6900, 1993.
[20] R. C. Spitzer, R. L. Kauffman, T. Orzechowski, D. W. Phillion, and C. Cerjan, "Soft x-ray production from laser produced plasmas for lithography applications," *J. Vac. Sci. Technol. B,* vol. 11, no. 6, pp. 2986–2989, 1993.

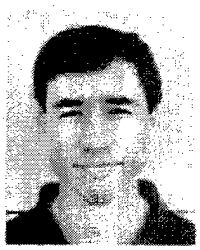

Tasshi Dennis received the B.A. degree in mathematics/physics from Whitman College, Walla Walla, WA, and, the B.S. degree in electrical engineering from the California Institute of Technology, Pasadena, CA, both in 1993, and the M.S. degree in electrical engineering from Rice University, Houston, TX, in May 1995.

He is currently doing research at Rice Univ. on code-division multiple-access optical-fiber communication.

Hendrik Matthew Duiker received the B.S. degree in electrical engineering from the California Institute of Technology, Pasadena, CA, in 1984, and the Ph.D. degree in physics from the University of Colorado, Boulder, CO, in 1989.

Jun Wu, photograph and biography not available at the time of publication.

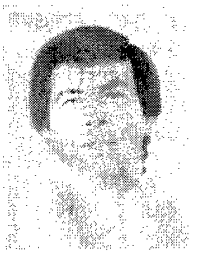

Csaba Tóth was born in Hungary, in 1959. He received the M.S. and Ph.D. degrees in physics from the Roland Eötvös University, Budapest, Hungary, in 1983 and 1986, respectively.

He has been working in the Research Institute for Solid-State Physics of the Hungarian Academy of Sciences, Budapest, since 1983, where he is presently a senior scientific coworker. In addition, he has been a visiting scientist at both the Research Center of Crete, Iraklion, Greece (1987 and 1990) and Rice University, Houston, TX (1993 and 1995). His experience is connected with mode-locked solid-state lasers, generation of ultrashort light pulses, excitation of ionic excimer molecules and extreme ultraviolet lasers by soft X-rays, and investigation of multiphoton interaction processes at metal surfaces.

Dr. Tóth is a member of the Hungarian Physical Society, the SPIE, and the Quantumelectronics Division of the European Physical Society.

James F. Young (M'72–SM'92) received the B.S. and M.S. degrees in electrical engineering from the Massachusetts Institute of Technology, in 1965 and 1966, and the Ph.D. degree in electrical engineering from Stanford University, in 1970.

He is a professor at Rice University in the Electrical and Computer Engineering Department. In addition to teaching undergraduate and graduate courses, he directs a research program concentrating on optical communication networks and on the development and application of extreme ultraviolet lasers. In 1975, he was appointed Research Professor of Electrical Engineering at Stanford University, and taught graduate courses in lasers, directed graduate student research, advised undergraduates, and served administrative capacities. His research topics included optical parametric oscillators, nonlinear optics in crystals and vapors, infrared image up conversion, and the development of unique laser sources, including femtosecond, terawatt lasers. He joined the Rice University faculty in 1990.

Dr. Young is a fellow of the Optical Society of America and a member of Tau Beta Pi Engineering Honor Society. He received the Stanford Electrical Engineering Department Outstanding Service Award, in 1985, and was named Stanford Master Advisor, in 1988, in recognition of his service to undergraduates. He was chosen as an IEEE Lasers and Electro-Optics Society Distinguished Lecturer, for 1991–1992. He has authored more than 70 publications, has served as a consultant to several companies, and has supervised the research of more than 30 graduate students.

PROCEEDINGS REPRINT

SPIE—The International Society for Optical Engineering

Reprinted from

National Science Foundation (NSF) Forum on Optical Science and Engineering

11–12 July 1995
San Diego, California

Volume 2524

Vacuum ultraviolet optical microscopy

J. F. Young H. M. Duiker I. Ferincz
T. Dennis

Department of Electrical and Computer Engineering,
and the Rice Quantum Institute,
Rice University, P.O. Box 1892, Houston, TX 77251
Phone: (713) 527–4721; FAX: (713) 524–5237; young@rice.edu

ABSTRACT

Microscopy using vacuum ultraviolet and soft x-ray radiation offers high resolution, high contrast, and chemical sensitivity. Holography and contact printing are unique in their potential to achieve wavelength-limited resolution because they eliminate optical elements and their imperfections. Both methods, however, lack magnification and require high resolution films and methods to recover images. We present our results on source development and film characterization.

Keywords: microscopy, vacuum ultraviolet, xenon laser.

1 INTRODUCTION

Short wavelength optical sources, particularly coherent sources, have long fascinated the scientific community, and extensive research has been done in the field during the last two decades. Much of the scientific interest stems from the challenges involved in realizing such sources, but the motivation is also based on the utility of short wavelength sources as tools to investigate new scientific areas and to solve technical problems. A commonly cited application for vacuum ultraviolet (VUV) and soft x-ray sources is high resolution imaging or microscopy: since the resolution of a conventional imaging system is limited to the wavelength of the illuminating source, shorter wavelength sources allow higher resolution images.

While the physical validity of the above statement is unassailable, it fails to address a number of practical issues. First, is it possible to design, even on paper, an optical imaging system that exploits extremely short wavelength sources; that is, a general imaging technique that can achieve *wavelength-limited resolution*, and that does so *independent of the wavelength* of the illuminating source? Second, if we do build such a system, will anyone care; will it satisfy a real need? One must keep in mind that there is a competing technology: electron microscopes provide resolution far above what optical systems will ever achieve, and they are commercial, convenient instruments. Furthermore, recent advances in near-field optical probes have demonstrated sub-wavelength resolution using apertures smaller than the illuminating wavelength.

Resolution, however, is only one parameter of an imaging system. The other major parameter, and one that is often more important, is *contrast*. Contrast results from variations in absorption, scattering, phase, refraction,

0-8194-1883-8/95/$6.00

etc., between different elements of the object, and is a function of both the sample and the illuminating energy. Without contrast there is *no* image, regardless of the resolution capabilities of the system. Different imaging systems rely on different contrast mechanisms, and although there is no fundamental reason, it often seems that there is a trade-off between contrast and resolution in most systems. The electron microscope achieves the highest resolution but sacrifices contrast almost completely for most objects. Extensive sample preparation is necessary to provide contrast. It seems likely that an imaging system with a resolution exceeding that of visible microscopes, but requiring less sample preparation than the electron microscope, would be useful in several fields, including the life sciences. However, this will depend critically on whether such an instrument can provide unique, important information that is not available any other, more convenient way. It seems unlikely that this can be determined without developing and testing an instrument.

For an optical microscope, the illumination wavelength influences both resolution and contrast. In an ideal world the choice of illumination wavelength would be based solely on contrast—the optical properties of the object and its background—and the imaging system would provide diffraction limited resolution. If greater resolution were required, shorter wavelengths would have to be used at the cost of reduced contrast and increased energy irradiation of the object, or more complex sample preparation would be required to create artificial contrast. In reality, however, constraints such as source availability and practicality often intrude, or even dominate.

The goal of our National Science Foundation program is the development and application of short wavelength imaging techniques, both contact imaging using broad bandwidth incoherent sources and holography using coherent sources. In the following sections we will review these image formation methods and present recent results on source development and film characterization. For a general review of short wave length imaging see the article by Howells, Kirz and Sayre;[1] additional technical details can be found in the excellent collections *X-Ray Microscopy I, II, & III*.[2–4]

2 IMAGE FORMATION

Reflective and diffractive optics can be used to form VUV images, but their performance is a strong function of wavelength and of fabrication precision. Optical elements have never achieved wavelength-limited resolution at VUV wavelengths, so the most flexible imaging technique would use no optics. There are two image formation methods that do not require optical elements: contact printing, and holography. The resolution of all other methods is determined in practice not by wavelength, but by one's ability to fabricate and align mechanical components. Indeed, Gabor invented holography as a way of forming electron microscope images without using lenses. Baez first recognized the potential of the technique in the x-ray region, where good focusing elements were also unavailable.[5]

Both contact printing and holography are capable of diffraction-limited resolution; both have limitations and problems. High resolution contact printing[3,6] is simple but restricted to thin objects; holography[7] requires a coherent source. More importantly, both methods lack magnification, and require high resolution films plus a method to recover the image and provide magnification. We are using laser-produced plasmas as a broad bandwidth, intense source of VUV radiation for film characterization and, in future, for contact printing. An atomic force microscope is used to read the exposure information off the film surface. The historical disadvantage of holography is the need for coherent illumination, but recent demonstrations of soft x-ray lasers have reduced this obstacle in principle.[8–10] These systems, however, are large, expensive, single-event devices that presently exist only at national laboratories. While they are excellent candidates for taking images, they are difficult to use for developing an imaging technique. We propose to use the Xe Auger laser at 109 nm to develop holographic imaging, because it is a practical, laboratory-scale, high repetition rate, VUV source.[11]

3 XE VUV LASER

The 109 nm Xe^{2+} Auger laser is a promising practical source of VUV radiation because of its unique combination of high gain, efficiency, benign physical properties, and short wavelength. It is pumped by soft x-rays from a laser-produced plasma: photoionization of an inner shell $4d$ electron is followed by rapid, selective Auger decay to the upper laser level. The threshold for Xe $4d$ photoionization is 68 eV, with a peak cross section of $3 \times 10^{-17}\,cm^2$ at 100 eV and a full width at half maximum of about 40 eV.[12] In this range, the photoionization cross section for $4d$ inner electrons is about ten times larger than that for the outer $5s$, $5p$ electrons. The practicality of this pumping method, and of the Xe^{2+} laser, depends critically on the conversion efficiency of laser light into soft x-ray radiation with the required spectrum, since higher efficiency reduces the size and cost of the pumping laser system. VUV lasers are single-pass amplifiers seeded by spontaneous emission, with much of the gain length operating in the small-signal, exponential gain regime; thus, small improvements in pumping efficiency can yield large improvements in output power and overall efficiency.

Several plasma target materials have been used previously for the Xe^{2+} laser: tantalum, gold, stainless steel, and mercury.[13-16,11,17] However, since the pump laser energy, pulse length, and focused intensity on target vary considerably among these experiments, it is difficult to isolate the effect of the target material on Xe^{2+} laser performance. We present the first experiments that quantitatively compare cadmium, copper, gold, zinc, and stainless steel plasma targets for pumping the 109 nm Xe^{2+} Auger laser under identical experimental conditions.

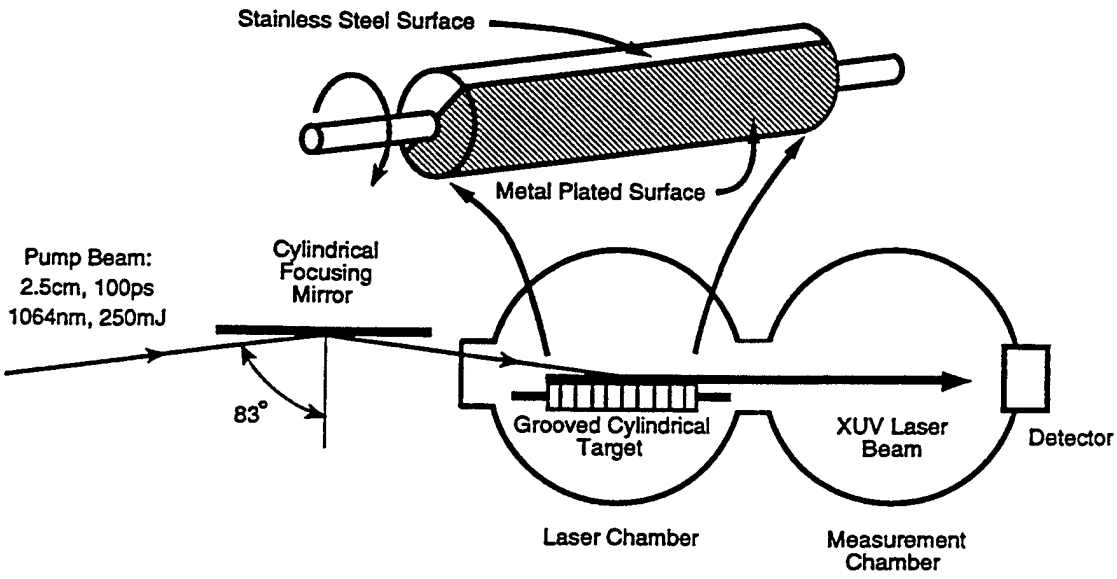

Figure 1: Target geometry for the 109 nm Xe^{2+} Auger laser.

The general pumping configuration has been described previously.[11] As shown in Fig. 1, the pump beam is focused to a $\sim 75\,\mu m$ wide by 20 cm long line on the grooved target using a cylindrical mirror at an 83 deg angle of incidence, resulting in a power density of about $10^{11}\,Wcm^{-2}$. The basic plasma target is a machined stainless steel rod 3.8 cm in diameter and 20 cm long, threaded at ~ 30 grooves per centimeter. The sample material was electroplated over half the circumference of the basic target, while the other half was left unplated to provide a reference signal from stainless steel. Targets were prepared using cadmium, copper, gold, and zinc. Rotation of the rod during laser operation exposed alternating sections of stainless steel and the plated sample material to the pump pulses.

The target rod is housed in a vacuum cell containing ~ 15 Torr of Xe gas. The output intensity of the forward propagating 109 nm beam was measured with an aluminum oxide cathode photodiode and oscilloscope. The length of the target pumped was varied using a moveable knife edge placed in the pump beam outside the target chamber. For each pumped length, the laser output energy was recorded for both the stainless steel and the plated metal regions as the target rotated. In this manner, data for the sample material and stainless steel were collected in alternating measurements while maintaining near-identical pumping conditions.

The data for the various target materials, are summarized in Table 1. We have observed a ~ 20% improvement in the gain coefficient and a ~ 112% improvement in total energy for a Xe^{2+} 109 nm laser by plating the stainless steel target with cadmium. Significant improvements in output using zinc and gold were also observed. Use of these targets for the Xe^{2+} laser can reduce the required pump energy or reduce exposure times for applications such as imaging or photochemistry. With a copper target, the 109 nm laser output exhibited large pulse-to-pulse fluctuations, with the best values only slightly larger than those for the stainless steel target. The fluctuations appeared to result from the presence of surface oxides and a more rapid copper surface ablation. The rapid generation of copper debris, coupled with only a minor improvement in output energy, make copper targets a poor choice for the Xe^{2+} 109 nm laser.

Material	Total output improvement	Small signal gain improvement
Cadmium	112%	20%
Zinc	100%	11%
Gold	100%	25%
Copper	25%	–

Table 1: Performance of target materials relative to stainless steel

It is reasonable to attribute the significant improvement in 109 nm laser output energy using a cadmium target to a higher pump to soft x-ray conversion efficiency, and/or to improved spectral properties. There are two plasma spectral factors that could be important. Increased plasma emission at 100 eV, overlaping the Xe inner shell $4d$ photoionization cross section, would enhance the production of the upper laser level; in contrast, increased output of low energy photons could reduce gain by ionizing the upper laser level to Xe^{3+} (requiring about 7 eV), or by ionizing neutral Xe (12.1 eV) and producing extra electrons, which are believed to quench the Xe^{2+} gain.[13] Although several authors report spectra of laser-produced plasmas for different target materials, the experimental conditions were generally quite different from those used for the Xe^{2+} laser, and low photon energy spectra were not measured. Thus, this data is of limited use in predicting target performance or in explaining our results.

In addition, it is simplistic to think that the plasma target material or atomic number is the only important parameter, or even an independent parameter. This is shown clearly in the work of Spitzer, et al.,[18] who made detailed spectral measurements of laser-produced plasma efficiency in the range of 50–250 eV for gold and tin targets. Both gold and tin have (at least local) emission peaks near 100 eV that match the Xe inner shell photoionization, so it is not surprising that we found gold to be a good target material. However, the pump conversion efficiency into the 80–150 eV band varies significantly with focal spot size and power density, and *the dependence is different for the two materials.*

Our work has shown that a simple change of target material can result in significant improvements in the Xe^{2+} 109 nm laser performance. At the same time, it is clear that we have explored only part of the full parameter space of target conditions, and our ranking of materials would probably change for different conditions of pump wavelength, pulse length, power density, and focal geometry. Our results represent a good starting point for a detailed optimization of pumping conditions in other situations.

4 HIGH RESOLUTION FILMS

The role of film in a short wavelength imaging system is identical to that in any other system: to record the incident intensity pattern accurately so that a faithful image may be recovered. Conventional photographic film is composed of individual photosensitive grains that act as amplifiers, and the highest resolution conventional films, with grains about 60 nm in diameter spaced about 200 nm apart, are inadequate for VUV high resolution imaging. It is necessary to employ a highly homogeneous recording medium.

One familiar form of grainless films are photoresists. Because of their technical importance for photolithography, a great deal of literature on their properties exists. The wavelengths used and the requirements of lithography, however, are quite different from imaging, and the available information is only partly relevant. One of the earliest and best characterized electron and x-ray resists is poly(methyl methacrylate), PMMA or plexiglas. Irradiation of PMMA causes scission of the chemical bonds joining the molecule, and a lower molecular weight region that dissolves more readily. The developed film consists of a pattern of surface relief corresponding to the exposure; we measure the resulting depth encoded image with our atomic force microscope (AFM). Our early work showed that PMMA is capable of recording high resolution VUV interference patterns,[19] but image recovery requires quantitative knowledge of the exposure response. The relationship between exposure and resulting surface depth is generally complex and little quantitative characterization of exposure response has been done. Research on this relationship is underway at several laboratories,[20] including ours.

A key factor determining response is the absorption of PMMA at the exposure wavelength. If the absorption is low, the light will pass through the PMMA layer with little effect, resulting in low sensitivity. If the absorption is very high, the light is confined to a thin surface layer, limiting the volume of photochemical reaction and the change of surface profile after development; the image will be lost in the noise. To date, the absorption of PMMA has been measured only down to about 150 nm, while our primary coherent exposure source is at 109 nm, the Xe III Auger laser. Our initial exposures of PMMA with 109 nm light resulted in very shallow surface features relative to exposures at other wavelengths, for example 118 nm.[19] Increasing the exposure flux level had little effect. Based on our experience and on previous measurements of the absorption of simple polymers, like paralodion, $C_{12}H_{16}(NO_2)_4O_6$,[21] we believe that the intrinsic absorption of PMMA increases significantly and sharply in the region around $\sim$ 100 nm. It is essential for this program that we determine the absorption characteristics of polymer films in the VUV; if all of them exhibit this sharp, large absorption feature, we will have to change to a different exposure wavelength and coherent source.

We have constructed a small laser-produced plasma light source to expose films and measure absorption over a wide range of wavelengths. One of the major problems has been to produce a bright source while reducing the effects of debris from the plasma. The plasma is also effectively an evaporation source that deposits target material on the light collection optics and spectrometer grating. While we have not eliminated the debris problem, we have reduced it sufficiently to permit practical operating times before cleaning or recoating optics. We are currently performing two types of experiments. We are directly measuring the absorption of PMMA films on a mirrored substrate using an interference fringe technique. We also making exposures of PMMA over a wide range of wavelengths and flux levels and measuring the resultant depth profiles with the AFM. While this is an indirect measure of absorption, it is the actual data we need to characterize the films for image reconstruction and selection of exposure wavelengths.

Unfortunately, PMMA is also known for its very low sensitivity. A more sensitive film would reduce source requirements and minimize radiation damage to the object. More sensitive polymers have been developed recently for short wavelength lithography, and they may prove useful for imaging applications.[22] This is an exciting research area, since the variety of polymer film compositions, the many processing options, and the complex dependence of sensitivity and accuracy parameters on the polymer chemistry mean that many trade-offs should be possible.

5 CONCLUSION

The VUV imaging system described above employs very sophisticated technology, and its development is a fascinating challenge that would have been unthinkable 25 years ago. It is possible now only because of technological advances in three areas: short wavelength sources, the atomic force microscope, and powerful desktop computers with sophisticated display capabilities.

Yet, a primary question remains unanswered: Can short wavelength microscopy reveal new information that is worth the complication and effort? Only time and experience will tell. We believe, however, that the quest may be as valuable as the goal, producing new scientific and engineering results applicable to many areas, along with the training of new scientists.

6 ACKNOWLEDGEMENTS

This work was jointly supported by the National Science Foundation (ECS–92–24628), the U.S. Air Force Office of Scientific Research (F49620–94–1–0017), and Rice University.

7 REFERENCES

[1] M. R. Howells, J. Kirz, and D. Sayre, "X-ray microscopes," *Scientific American*, pp. 88–94, Feb. 1991.

[2] G. Schmahl and D. Rudolph, eds., *X-Ray Microscopy*, vol. 43 of *Springer Series in Optical Sciences*. Springer-Verlag, 1984.

[3] D. Sayre, M. Howells, J. Kirz, and H. Rarback, eds., *X-Ray Microscopy II*, vol. 56 of *Springer Series in Optical Sciences*. Springer-Verlag, 1988.

[4] A. G. Michette, G. R. Morrison, and C. J. Buckley, eds., *X-Ray Microscopy III*, vol. 67 of *Springer Series in Optical Sciences*. Springer-Verlag, 1992.

[5] A. V. Baez, "A study in diffration microscopy with special reference to x-rays," *Journal of the Optical Society of America*, vol. 42, pp. 756–762, 1952.

[6] R. J. Rosser, K. G. Baldwin, R. Feder, D. Bassett, A. Coles, and R. W. Eason, "Soft x-ray contact microscopy with nanosecond exposure times," *Journal of Microscopy*, vol. 138, pp. 311–319, 1985.

[7] R. J. Collier, C. B. Burckhard, and L. H. Lin, *Optical Holography*. Academic Press, 1971.

[8] J. E. Trebes, S. B. Brown, E. M. Campbell, D. L. Matthews, D. G. Nilson, G. F. Stone, and D. A. Whelan, "Demonstration of x-ray holography with an x-ray laser," *Science*, vol. 238, pp. 517–519, 1987.

[9] D. L. Matthews and M. D. Rosen, "Soft x-ray lasers," *Scientific American*, pp. 86–91, Dec. 1988.

[10] S. Suckewer and C. H. Skinner, "Soft x-ray lasers and their applications," *Science*, vol. 247, pp. 1553–1557, 1990.

[11] T. S. Clement, C. Tóth, J. Wu, and J. F. Young, "A reasonably practical XUV laser for applications," *IEEE Journal of Quantum Electronics*, vol. 30, pp. 2136–2140, 1994.

[12] D. M. P. Holland, K. Codling, J. B. West, and G. V. Marr, "Multiple photoionization in the rare gases from threshold to 280 eV," *Journal of Physics B: Atomic and Molecular Physics*, vol. 12, pp. 2465–2484, 1979.

[13] H. C. Kapteyn and R. W. Falcone, "Observation of a short-wavelength laser pumped by auger decay," *Physical Review Letters*, vol. 57, pp. 2939–2942, 1986.

[14] G. Y. Yin *et al.*, "Low-energy pumping of a 108.9 nm xenon Auger laser," *Optics Letters*, vol. 12, pp. 331–333, 1987.

[15] M. H. Sher, J. J. Macklin, J. F. Young, and S. E. Harris, "Saturation of the Xe III 109 nm laser using traveling-wave laser-produced-plasma excitation," *Optics Letters*, vol. 12, pp. 891–893, 1987.

[16] M. H. Sher, S. J. Benerofe, J. F. Young, and S. E. Harris, "2-Hz 109 nm mirrorless laser," *Journal of the Optical Society of America B*, vol. 8, pp. 114–116, 1991.

[17] H. Yamakoshi, C. T. Chin, S. Jaimungal, P. R. Herman, F. Budnik, G. Kulesár, L. Zhao, and R. S. Majoribanks, "Extreme-ultraviolet laser photo-pumped by a self-healing Hg target," in *Applications of Laser Plasma Radiation*, vol. 2015, (Bellingham, WA 98227–0010), SPIE, 1993.

[18] R. C. Spitzer, R. L. Dauffman, T. Orzechowski, D. W. Phillion, and C. Cerjan, "Soft x-ray production from laser produced plasmas for lithography applications," *Journal of Vacuum Science and Technology B*, vol. 11, pp. 2986–2989, 1993.

[19] G. C. Bjorklund, S. E. Harris, and J. F. Young, "Vacuum ultraviolet holography," *Applied Physics Letters*, vol. 25, pp. 451–452, 1974.

[20] G. D. Kubiak *et al.*, "Resist charcterization at soft-x-ray wavelengths," in *OSA Proceedings on Soft-X-Ray Lithography* (J. Bokor, ed.), vol. 12, pp. 124–128, Optical Society of America, 1991.

[21] J. A. Samson, *Techniques of Vacuum Ultraviolet Spectroscopy*. Lincoln, Nebraska: Pied Publications, 1967.

[22] G. D. Kubiak, R. Q. Huang, M. T. Schulberg, D. A. Tichenor, and K. Early, "Chemically amplified soft-x-ray resists: Sensitivity, resolution, and molecular photodesorption," *Applied Optics*, vol. 32, pp. 7036–7043, 1993.

Systems and Applications

Continued

tions of high resolution integrated circuits and nanostructures.

A commonly cited application for vacuum ultraviolet (VUV) and soft x-ray sources is high resolution imaging or microscopy: since the resolution of a conventional imaging system is limited to the wavelength of the illuminating source, shorter wavelength sources allow higher resolution images. (For a general review, see [1]; details on the work discussed in this article can be found in the excellent collections of [2,3,4].) While the physical validity of this statement is unassailable, it fails to address a number of practical issues. First, is it possible to design, even on paper, an optical imaging system that exploits extremely short wavelength sources; that is, a general imaging technique that can achieve *wavelength-limited resolution,* and that does so *independent of the wavelength* of the illuminating source? Second, if we do build such a system, will anyone care; will it satisfy a real need? One must keep in mind that there is a competing technology; electron microscopes provide resolution far above what optical systems will ever achieve, and they are commercial, convenient instruments. Furthermore, recent advances in near-field optical probes have demonstrated sub-wavelength resolution using apertures smaller than the illuminating wavelength. So, do short wavelength imaging systems really have anything to offer? The answer is unclear at present, and a simple answer will probably never be possible, making this an interesting field. This article will explore, briefly and incompletely, these issues.

2 Imaging Issues

Resolution is only one parameter of an imaging system. The other major parameter, and one that is often more important, is *contrast.* Contrast results from variations in absorption, scattering, phase, refraction, etc., between different elements of the object, and is a function of both the sample and the illuminating energy. Without contrast there is *no* image, regarding less of the resolution capabilities of the system. Different imaging systems rely on different contrast mechanisms, and although there is no fundamental reason, it often seems that there is a trade-off between contrast and resolution in most systems. Thus, there is no single best or perfect microscopic imaging technique, and microscopists often use several to examine an object. Each approach makes different compromises, optimizes different parameters, and provides different types of information. The electron microscope achieves the highest resolution but sacrifices contrast almost completely, at least for biological materials. The extensive processing required to provide contrast for high energy electrons often raises questions about whether details in the final image are due to the *sample* or to the sample *preparation.* It seems likely that an imaging system with a resolution exceeding that of visible microscopes, but requiring less invasive sample preparation than the electron microscope, would be useful in several fields, including the life sciences. However, this will depend critically on whether such an instrument can provide unique, important information that is not available any other, more convenient way. Unfortunately, it seems unlikely that this can be determined without developing and testing an instrument.

For an optical microscope, the illumination wavelength influences both resolution and contrast. In an ideal world (see Fig. 1), the choice of illumination wavelength would be based solely on contrast—the optical properties of the object and its background—and the imaging system would provide diffraction limited resolution. If greater resolution were required, shorter wavelengths would have to be used at the cost of reduced contrast and increased energy irradiation of the object, or more complex sample preparation would be required to create artificial contrast. This optimum strategy requires a very general, flexible imaging approach; one which is largely wavelength independent, with wavelength-limited resolution. In reality, however, constraints such as source availability and practicality often intrude, or even dominate. A flexible, high resolution technique is even more essential to avoid adding further constraints.

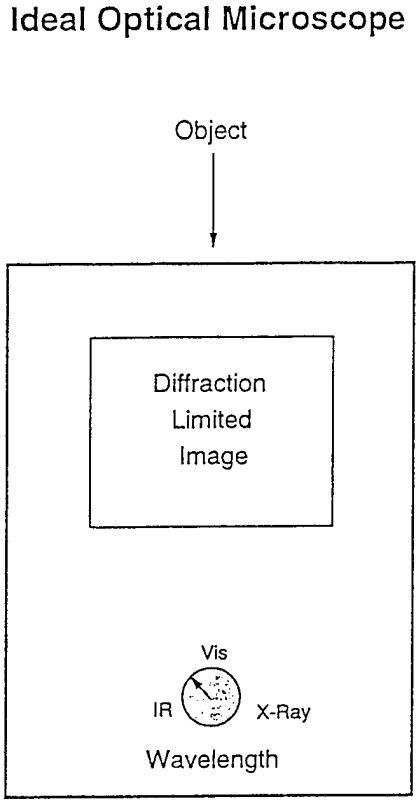

Figure 1: User's conception of the ideal microscope; insert sample, pick wavelength, and view diffraction limited image.

There are three general, interrelated issues in building an instrument approaching that in Fig. 1: the image formation method or optics; the radiation source; and the image recording/recovery method. The discussion below concentrates on image formation and the choice of wavelength.

3 Image Formation

Reflective and diffractive optics can be used to form VUV images, but their performance is a strong function of wavelength and of fabrication precision. Optical elements have never achieved wavelength-limited resolution at VUV wavelengths, so the most flexible imaging technique would use no optics. There are two image formation methods that do not require optical elements: contact printing, and holography. The resolution of all other methods is determined in practice not by wavelength, but by one's ability to fabricate and align mechanical components. Indeed, Gabor invented holography as a way of forming electron

Continued on page 8

Continued

microscope images without using lenses. Baez first recognized the potential of the technique in the x-ray region, where good focusing elements were also unavailable.[5]

Both contact printing and holography are capable of diffraction-limited resolution; both have limitations and problems. High resolution contact printing is simple but restricted to thin objects; holography requires a coherent source. More importantly, both methods lack magnification, and require high resolution films plus a method to recover the image and provide magnification. The image recovery/magnification method cannot be optically based, or we return to the original resolution problem.

Contact microradiography using x-ray tubes, pulsed discharges, laser-produced plasmas, or synchrotron sources is a well developed technique that is widely used in a number of fields.[3, pages 46-49][6] Careful choice of wavelength provides good contrast and even chemical sensitivity. The use of new pulsed sources has eliminated previous problems of motion during long exposures, but the resolution of thick samples is still spoiled by diffraction.

Holography is a technique for recording the amplitude and phase of a wavefront of coherent radiation, such as that passing through an object, by recording the amplitude of the interference pattern between that wavefront and a reference wavefront.[7] For imaging small objects, the simple, in-line, far-field, Fraunhofer geometry shown in Fig. 2 is particularly appropriate. The interference takes place between light scattered by the object, and the object is placed in the far-field of the object. Not even a beamsplitter is required. The physical scale of this geometry is surprising. For an object diameter of $2\,\mu m$, the required far-field distance to the film is only about $z_0 = 50\,\mu m$, even for a wavelength of 100 nm. If the object were an amplituted grating with light and dark fringes separated by the illuminating wavelength, light would be diffracted from the input beam at angles $\pm \pi/4$, and the diameter of the hologram would thus be about $100\,\mu m$. These are very small holograms. In fact, it is hard to find these microscopic, transparent exposures on a large film surface.

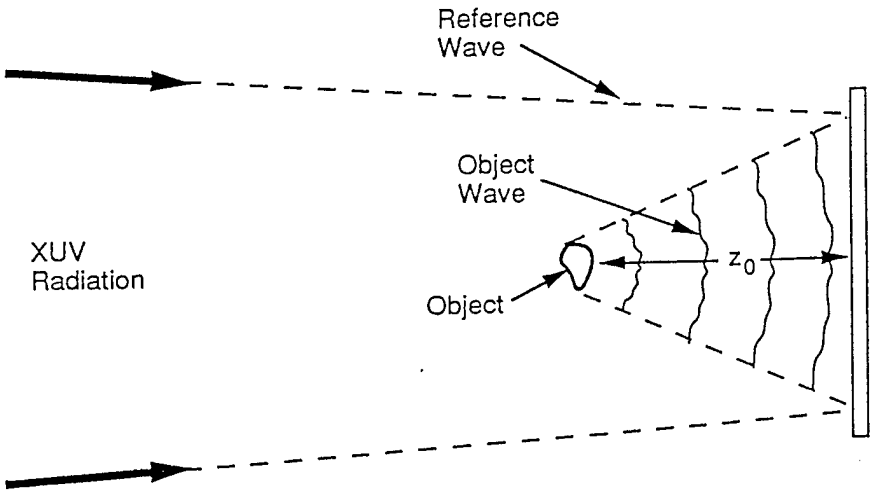

Figure 2: The in-line, far-field Fraunhofer hologram geometry.

The historical disadvantage of holography is the need for coherent illumination, but recent demonstrations of soft x-ray lasers have removed this obstacle, in principle if not in practice.[8,9,10] Practical, laboratory-scale, high repetition rate, VUV lasers are now available for system development and demonstration,[11] and advances at shorter wavelengths are imminent. The source energy and spatial coherence requirements are low for the in-line geometry because the areas are small; the temporal coherence requirement is low because the maximum path length difference between the scattered wave and the reference beam is also small. In fact, such holograms can be made with suitably filtered, non-laser sources, such as undulators. See pages 318-335 of [2], pages 253-262 of [3], and [4].

While the above arguments are true in principle, I want to emphasize that the best short wavelength imaging to date has been done using optical elements. For current examples of soft x-ray achievements, see Parts V & VI of [4]. Those results will be hard to match. (The observant reader will note that this article does not include any microscopic images.) Advantages in the fabrication of micro-zone Fresnel lenses and multilayer reflectors have led to significant improvements in imaging and scanning microscopes. [3, pages 310-315] [12,13,14,15] Particularly impressive is the Fresnel lens, soft x-ray microscope developed by Gunter Schmal's group, using an undulator at the BESY facility.[12][4, pages 392-396, and 404-407] Similar work is underway at Brookhaven [3, pages 253-262], Princeton[10], and the new Advanced Light Source at Lawrence Berkeley Laboratory.[16] The resolution of a Fresnel lens is determined by the thinest zone that can be reliably fabricated, currently about 30 nm. This will undoubtedly improve, but will probably always be significantly less than the limit imposed by the illuminating wavelength.

4 Choice of Wavelength

The unique feature of short wavelength microscopes is clearly the wavelength; does it provide improved contrast? For biological objects there has been considerable emphasis on the advantage, even the necessity, of using radiation near the "water window," the spectral region where water is reasonably transparent but carbon is not, about 2.3 nm to 4.3 nm. Detailed calculations by London, Rosen, and Trebes[17] of the optical properties of representative biological materials indicate that the optimum contrast for holography occurs for wavelengths somewhat longer than the water window edge. Incoherent sources in this region are available and reasonably convenient. Coherent sources have been produced,[18] but they are large, expensive, single-event devices that presently exist only at national laboratories.

However, the water window contrast criteria, while certainly valid and impor-

Continued on page 9

Continued

tant, is neither universal nor unique. Most obviously, not all interesting objects are biological and/or wet. But even for biological samples, there is another issue. Very short wavelength radiation interacts only with the inner shell electrons of an atom; the exact structure and the local environment do not effect the contrast. Thus, while radiation in the water window provides excellent discrimination between *water* and biological materials, it provides almost no contrast between *different* biological materials—lipid, protein, nucleosome, or DNA—because their atomic compositions are nearly identical.

But in many applications a sensitivity to molecular structure, binding, or surrounding is critical, and this requires a probe wavelength that interacts with the outer, valence electrons. Maximum contrast can be expected to occur for radiation near the ionization or dissociation limit of molecules and atoms. The first ionization limit of common elements all fall in the VUV, as shown in Fig. 3. Because of resonances, optical properties in this region will be a sensitive function of the atomic composition, the specific nature of the molecule composed of those atoms, its surrounding environment and bonding, and the illuminating wavelength.

This qualitative argument suggests that microscopy using light in the 200 nm to 50 nm range should provide unique information about biological objects with a minimum of preparation. This is fortunate because most of the practical, accessible, VUV sources emit in this same region. Unfortunately, quantitative data to support this argument is unavailable. The optical properties of biological materials, or even of organic liquids, have not been measured in the spectral region, and the interactions are too complex to calculate even roughly. It may be that the absorptions in this spectral region are too extensive, and that no spectral regions of sufficient transparency for good imaging exist. Certainly water is very absorbing, and reasonably dry samples will be required. Simple drying is not a particularly severe preparation procedure, but it eliminates the possibility of imaging live cells. Good experimental data is needed to assess the practicality of imaging in this wavelength region.

5 High Resolution Films

The role of film in a short wavelength imaging system is identical to that in any other system: to record the incident intensity pattern accurately so that a faithful image may be recovered. Conventional photographic film is composed of individual photosensitive grains that act as amplifiers, and the highest resolution conventional films, with grains about 60 nm in diameter spaced about 200 nm apart, are inadequate for VUV high resolution imaging. It is necessary to employ a highly homogeneous recording medium.

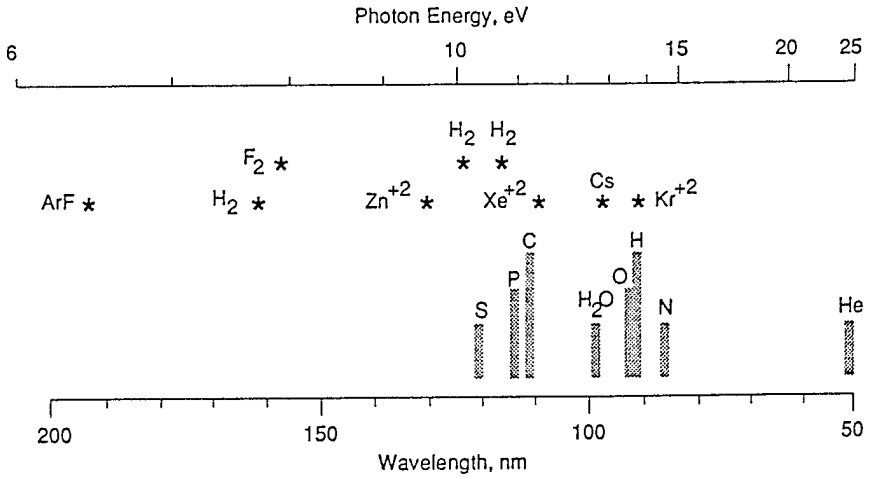

Figure 3: Ionization limits of some common elements (bars), and VUV laser wavelengths (stars).

Grainless films are undoubtedly familiar to LEOS members in the form of photoresists. Because of their technical importance for photolithography, a great deal of literature on their properties exists. The wavelengths used and the requirements of lithography, however, are quite different from imaging, and the available information is only partly relevant. For example, data on microfiche films are not very useful in choosing a film to photograph a Monet painting. One of the earliest and best characterized electron and x-ray resists is poly(methyl methacrylate), PMMA or plexiglas. Irradiation of PMMA causes scission of the chemical bonds joining the molecule, and a lower molecular weight region that dissolves more readily. The developed film consists of a pattern of surface relief corresponding to the exposure, but the relationship is generally complex and not well known. Research on this relationship is underway at several laboratories,[19] including ours. Our early work showed that PMMA is capable of recording high resolution VUV interference patterns.[20]

Unfortunately, PMMA is also known for its very low sensitivity. A more sensitive film would reduce source requirements and minimize radiation damage to the object. More sensitive polymers have been developed recently for short wavelength lithography, and they may prove useful for imaging applications.[21] This is an exciting research area, since the variety of polymer film compositions, the many processing options, and the complex dependence of sensitivity and accuracy parameters on the polymer chemistry mean that many trade-offs should be possible.

6 Image Recovery

Following film exposure and development, the resulting contact print or hologram may contain spatial frequency components up to $1/\lambda$: too high to be resolved and enlarged using visible optical instruments. The patterns can be seen using a scanning electron microscope, but it does not provide a quantitative map of surface height. Quantitative measurement of the surface depth pattern using transmission electron microscopy, which certianly has adequate transverse resolution, is hampered by a lack of contrast, as usual. Nevertheless, holograms have been measured this way and images reconstructed numerically.[3, pages 253-262]

Continued on page 12

Continued

Technological advances now provide a convenient alternative: the atomic force microscope (AFM). These instruments routinely measure surface topology with resolution exceeding a nanometer. They can measure polymer surfaces directly, without preparation. Yet, commercial AFMs are not a complete solution. First, image reconstruction will require larger data sets than present instruments can handle. A second, more serious, shortcoming of current AFMs is poor absolute position accuracy on long scans. For holography, inaccuracies result in phase errors that reduce the coherence of the data and degrade the reconstructed image. The accuracy of AFMs is improving rapidly, but it may be necessary to add independent, high resolution spatial position sensors, such as a laser interferometer, to the AFM, and to integrate it into the external data collection system. Contrast print readout is not as critical and requires much less accuracy; current instruments are adequate.

Once a digital map of a contact print or hologram is stored in the computer, the numerical processing is relatively straightforward. Numerical reconstruction will allow us to compensate for film and AFM readout characteristics during the calculations. Additional image processing during reconstruction may ultimately offer the most dramatic opportunities for advancements in the function and scientific utility of this imaging technique. It seems likely that new types of image enhancement will be possible for microscopic biological objectives using the measured properties of different biological materials. The development of a convenient user interface and of specialized displays also offers exciting potential.

7 Conclusion

The "microscope" described above certainly bears little resemblance to the one I used in school. It employs very sophisticated technology, and its development is a fascinating challenge that would have been unthinkable 25 years ago. It is possible now only because of technological advances in three areas: short wavelength sources, the atomic force microscope, and powerful desktop computers with sophisticated display capabilities.

Yet, my primary question remains unanswered: Can short wavelength microscopy reveal new information that is worth the complication and effort? Only time and experience will tell. I believe, however, that the quest may be as valuable as the goal, producing new scientific and engineering results applicable to many areas, along with the training of new scientists. I hope my research sponsors (the National Science Foundation, the U.S. Air Force Office of Scientific Research, and Rice University) also still believe that after reading this article.

8 Disclaimer

This may look like a review article, but it is not. There are many aspects of the VUV imaging problem, and alternative solutions, that I have not covered. The selection has been very personal. I apologize to the many workers whose advances I have not mentioned, and I apologize to those whose work I have mentioned but inadequately referenced. I am sure the editor will welcome submissions on related issues.

References

[1] M.R. Howells, J. Kirz, and D. Sayre, "X-ray microscopes," *Scientific American*, pp. 88-94, Feb. 1991.

[2] G. Schmahl and D. Rudolph, eds., *X-Ray Microscopy*, vol. 43 of *Springer Series in Optical Sciences*. Springer-Verlag, 1984.

[3] D. Sayre, M. Howells, J. Kirz, and H. Rarback, eds., *X-Ray Microscopy II, vol. 56 of Springer Series in Optical Sciences*. Springer-Verlag, 1988.

[4] A. G. Michette, G. R. Morrison, and C. J. Buckley, eds., *X-Ray Microscopy III*, vol. 67 of *Springer Series in Optical Sciences*. Springer-Verlag, 1992.

[5] A.V. Baez, "A study in diffration microscopy with special reference to x-rays," *Journal of the Optical Society of America*, vol. 42, pp, 756-762, 1952.

[6] R. J. Rosser, K. G. Baldwin, R. Feder, D. Bassett, A. Coles, and R. W. Eason, "Soft x-ray contact microscopy with nanosecond exposure times," *Journal of Microscopy*, vol. 138, pp. 311-319, 1985.

[7] R.J. Collier, C.B. Burckhard, and L.H. Lin, *Optical Holography*. Academic Press, 1971.

[8] J. E. Trebes, S. B. Brown, E. M. Campbell, D. L. Matthews, D. G. Nilson, G. F. Stone, and D. A. Whelan, "Demonstration of x-ray holography with an x-ray laser," *Science*, vol. 238, pp. 517-519, 1987.

[9] D. L. Matthews and M. D. Rosen, "Soft x-ray lasers," *Scientific American*, pp. 86-91, Dec. 1988.

[10] S. Suckewer and C. H. Skinner, "Soft x-ray lasers and their applications," *Science*, vol. 247, pp. 1553-1557, 1990.

[11] T.S. Clement, C. Toth, J. Wu, and J.F. Young, "A reasonably practical XUV laser for applications," *IEEE Journal of Quantum Electronics*, (to be published).

[12] G. Schmahl, D. Rudolph, B. Niemann, and O. Christ, "Zone-plate x-ray microscopy," *Quart, Rev. Biophysics*, vol. 13, pp. 297-315, 1980.

[13] J. M. Kenney, C. Jacobson, J. Kirz, H. Rarback, F. Cinotti, W. Thomlinson, R. Rosser, and G. Schidlovsky, "Absorption microanalysis with a scanning soft x-ray microscope," *Journal of Microscopy*, vol. 138, p. 321, 1985.

[14] M. Kado, K. A. Tanaka, R. Kodama, T. Yamanaka, S. Nakai, K. Yamashita, M. Ohtani, and S. Kitamoto, "Development of a schwarzschild-type x-ray microscope," *Optics Letters*, vol. 16, pp. 109-111, 1991.

[15] H. Rarback, D. Shu, S. C. Feng, H. Ade, J. Kirz, I. McNulty, D. P. Kern, T. H. P. Chang, Y. Vladimirsky, N. Iskander, D. Attwood, K. McQuaid, and S. Rithman, "Scanning x-ray microscope with 75-nm resolution," *Rev. Sci. Instrum.*, vol. 59, pp. 52-59, 1988.

[16] D. Attwood, "New opportunities at soft-x-ray wavelengths," *Physics Today*, pp. 24-31, Aug. 1992.

[17] R. A. London, M. D. Rosen, and J. E. Trebes, "Wavelength choice for soft x-ray laser holography of biological samples," *Applied Optics*, vol. 28, pp. 3397-3404, 1989.

[18] L. B. DaSilva *et al.*, "Demonstration of x-ray microscopy with an x-ray laser operating near the carbon K edge," *Optics Letters*, vol. 17, pp. 754-756, 1992.

[19] G.D. Kubiak *et al.*, "Resist characterization at soft x-ray wavelengths," in *OSA Proceedings on Soft-X-Ray Lithography* (J. Bokor, ed.), vol. 12, pp. 124-128, Optical

Continued on page 15

Society of America, 1991.
[20] G. C. Bjorklund, S. E. Harris, and J. F. Young, "Vacuum ultraviolet holography," *Applied Physics Letters*, vol. 25, pp. 451-452, 1974.
[21] G. D. Kubiak, R. Q. Huang, M. T. Schulberg, D. A. Tichenor, and K. Early, "Chemically amplified soft-x-ray resists: Sensitivity, resolution, and molecular photodesorption," *Applied Optics*, vol. 32, pp. 7036-7043, 1993.

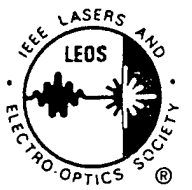

1. LASER-PRODUCED PLASMAS AS SHORT-WAVELENGTH INCOHERENT OPTICAL SOURCES

James F. Young

Department of Electrical and Computer Engineering,
Rice University
Houston, Texas

1.1 Introduction

Incoherent sources are useful experimental tools that have long been used throughout the optical spectrum, subject to availability. Recent technological advances have extended the available range into the vacuum ultraviolet and soft x-ray range through the use of laser-produced plasmas. This chapter will concentrate on the description of these new sources. Traditional vacuum ultraviolet sources and appropriate experimental techniques in this spectral range have been discussed in detail previously [1]. Conventional sources in other spectral regions—from the infrared, through the visible, to the ultraviolet quartz absorption edge at about 160 nm—have also been reviewed [2].

Figure 1 shows a typical configuration of a laser-produced plasma. A pulsed high-power laser is focused to a small spot on a metal target. A small, hot, radiating plasma or spark is formed that is characterized by very high densities of electrons and ions, very large density gradients, and very high temperatures. The parameters can be comparable to those in stellar interiors. Much of the work on laser-produced plasmas was motivated by the laser inertial confinement fusion program, and therefore concentrated on low-atomic-number targets irradiated at extremely high power densities, perhaps 10^{15} W cm^{-2}; interest was focused on shock wave formation, ablation rates, and radiation above 1 keV [3, 4]. Researchers in other fields, however, realized that laser-produced plasmas could be produced at much lower laser fluences, and therefore with smaller, practical lasers, and yet still provide unique sources of short-wavelength radiation [5–18]. Laser-produced plasmas can be used as a point source to illuminate a separate sample, but often, as shown in Fig. 1, a gas of the atoms to be irradiated surrounds the plasma, eliminating collection optics. The combination of a laser-produced plasma and a surrounding gas that can be photoionized also represents a unique pulsed source of hot electrons that can be used to excite optically forbidden transitions [19, 20]. Even a modest pumping laser can produce an effective electron current density of $>10^5$ A-cm^{-2} with a subnanosecond rise time.

EXPERIMENTAL METHODS IN THE PHYSICAL SCIENCES
Vol. 29C

1079-4042/97 $25.00

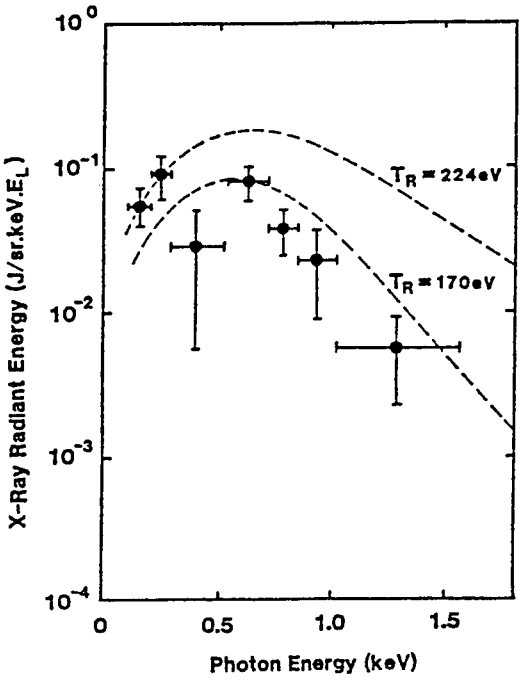

FIG. 2. Radiant energy spectra from an Au target illuminated by a 100-psec 530-nm pulse focused to 4×10^{14} W cm^{-2}. The dashed lines show black-body radiation spectral profiles for the indicated temperatures. From reference [51]. Reprinted with permission from the American Institute of Physics.

to several keV. Figure 2 shows a comparison between measured radiant energy spectra from an Au target and calculated black-body radiation spectral profiles. The agreement is reasonably good, but the black-body temperature of a laser-produced plasma, although useful, should be used only qualitatively. The conversion efficiency from input laser energy to total energy radiated by a plasma can vary from a few percent to more than 60%, as shown in Fig. 3 [21]. These data also show the advantages of short-wavelength pump lasers. The time behavior of the plasma temperature and radiation generally follows that of the driving laser pulse, at least down to about 10-ps time scales, providing a unique tool for time-resolved studies [22–25].

Before reviewing the characteristics of black-body radiators and summarizing the physics of laser-heated plasmas, it is helpful to present some typical numbers to place laser-produced plasmas in a physical context. High focused light intensities are required to initiate and sustain a plasma. While densities of 10^{15} W cm^{-2} and higher have been used to produce high x-ray yields, typical values for laboratory sources are 10^{11} to 10^{13} W cm^{-2}. Thus, for a focal spot of 50 μm diameter, a

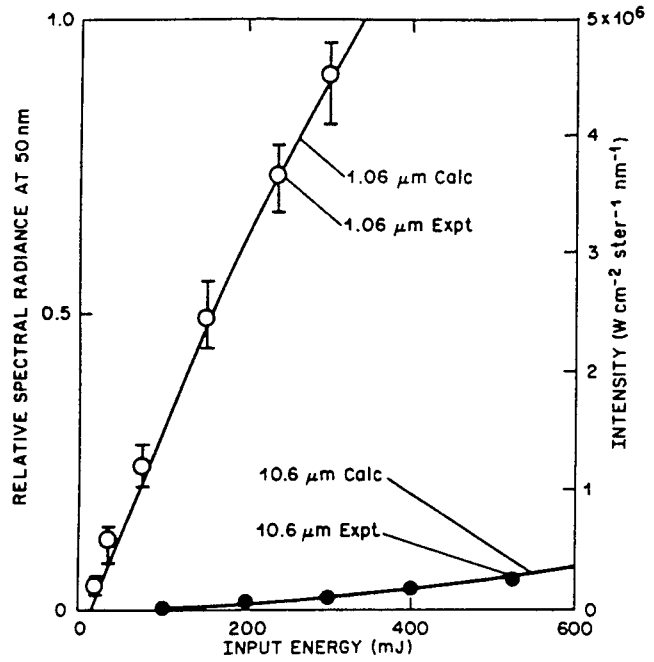

FIG. 4. Spectral radiance at 50 nm as a function of pump input energy for 1064 nm (○) and 10.6 nm (●). The solid curves are theoretical calculations. From reference [27]. Reprinted with permission from the Optical Society of America.

Although Nd Q-switched lasers with pulse lengths up to 10 nsec are used to heat plasmas, Nd mode-locked lasers with pulse lengths of about 100 psec are used more often. Minimum required pulse energies are therefore in the range of 1 to 200 mJ. The recent commercial availability of such sources with high repetition rates has made laser-produced plasmas practical experimental light sources. Ultrashort subpicosecond pulse length laser systems based on dye or Ti:sapphire gain media have been used to produce plasmas with unique characteristics [29–34]. The plasmas produced by very short high-intensity pump pulses are fundamentally different from those produced by more conventional pump sources, which are discussed here. For example, Fig. 5 shows the high-energy spectrum radiated by a plasma heated by a 0.5-TW 120-fsec pulse focused to a density greater than 10^{18} W cm^{-2}. Hard x-ray radiation extending beyond 1 MeV was observed. The spectrum was taken through 19 mm of lead to avoid saturating the detector. The physics of plasma formation and heating under such conditions are quite different from that presented here and are still an active area of research.

Although the dependence of the black-body spectral radiance on source temperature (Eq. 1) is quite familiar, it is worth repeating that, as the temperature is raised, not only does the peak emission shift to shorter wavelengths, but the emission at *every* wavelength also increases. Thus, for such sources hotter is always better, in terms of spectral radiance, although in some cases it may be advantageous to tune the emission peak to the wavelength of experimental interest in order to minimize the variation of spectral radiance with wavelength.

The wavelength of maximum spectral radiance is

$$\lambda_{max}(T) = 249.9/T \text{ nm}, \tag{2}$$

and the radiance at the peak is

$$W_{max}(T) = (2.873 \times 10^6)T^5 \text{ W cm}^{-2} \text{ s}^{-1} \text{ nm}^{-1}. \tag{3}$$

The total output flux of a black-body radiator can be found by integrating Eq. (1):

$$W_{total}(T) = \int_0^\infty W(\lambda,T)\, d\lambda = 32{,}650\, T^4 \text{ W cm}^{-2} \text{ sr}^{-1}, \tag{4}$$

which is known as the Stefan–Boltzmann law. Tabulations of these functions, along with integrals of the spectral radiance over finite intervals, are available [35].

It is possible to construct good approximations to low-temperature black-body sources using heated elements, and they are often used in the infrared. But conventional sources with constant temperatures above about 2000 K or $T = 0.17$ eV, corresponding to an emission maximum at 1450 nm, are impractical. Experiments at short wavelengths require a source with an effective temperature at least 100 times higher.

Sources of all types are often described as being effective black-body radiators or as having a particular black-body temperature, but the meaning of these designations is nonstandard and often unclear. An effective black-body temperature may be assigned based on Eq. (2) or (3) using measured values of the source's peak radiance or the wavelength of maximum spectral radiance, even though the wavelength dependence of the source radiance fails to match Eq. (1) very closely. Sometimes it means only that the source has a broad bandwidth relative to the application requirements and a smoothly varying spectral profile. Laser-produced plasma sources are often modeled as a black-body source characterized by an effective temperature. It is a useful qualitative description but is rarely accurate over a broad range. It does, however, have the considerable practical advantages of being easy to explain and easy to use in estimates of flux levels.

1.3 Laser-Produced Plasmas

It is not possible to provide a comprehensive review of laser–plasma interactions here. The subject is far too extensive and complex, and is the focus of much

In the plasma corona, the spatial gradient, or scale length, of the plasma electron density is usually determined by the dynamics of the plasma expansion, since electron and ion temperature gradients are small and have little physical effect. During short laser pulse lengths the plasma expands a distance much less than the focal spot diameter, and the electron density scale length is roughly $L_e = \tau v_p$, where τ is the pulse length. For long pulse lengths or in the limit of very small focal spots, however, the plasma isodensity contours are determined by the geometrical divergence of the plasma flow and are nonplanar, as illustrated in Fig. 6. Thus, if the product τv_p is larger than the focal spot diameter, then the scale length L_e will be reduced to approximately the focal spot radius. There are two reasons to operate in a regime of planar geometry that maximizes L_e. First, the analysis is simpler and the results are likely to be more reasonable; we assume a planar geometry in all the following calculations. Second, as we will show later, the laser energy absorbed by the plasma increases rapidly with L_e. Practically, however, it may be difficult to operate in the planar regime when using long laser pulses, because the required laser energy increases as τ^3 for fixed focal intensity.

The primary heating mechanism in laser-produced plasmas of interest here is inverse Bremsstrahlung, or collisional absorption. Each electron in the optical electric field $\mathcal{E}$ experiences a periodic acceleration that drives an oscillatory motion. Within a few optical cycles, this quiver motion reaches steady state, and the electron acquires an average energy of

$$E_p = \frac{e^2 \mathcal{E}^2}{2m\omega^2} = 10^{-7} I \lambda^2 \text{ eV} \tag{7}$$

in addition to its thermal energy, where I is the laser intensity in watts per square centimeter. If the electron suffers a dephasing collision with an ion while it is oscillating, the associated ponderomotive (or quiver) energy E_p is transferred permanently from the field to the electron. Thus, the average electron heating rate is equal to the product of E_p, the electron density, and the electron–ion collision frequency, which is also proportional to the electron density. Most of the plasma heating therefore takes place in the vicinity of n_C, the highest electron density the field can penetrate. Figure 7 is a schematic of a laser-produced plasma indicating this geometry.

The fraction of laser energy absorbed as the light propagates into the plasma to the critical density surface and back out depends on the shape of the density profile and the angle of incidence. The electron density profile of the coronal plasma is often modeled as $n_e(z) = n_C \exp(-z/L_e)$, in which case the fractional absorption is:

$$F = 1 - \exp\left(\frac{8\nu_C L_e}{3c}\cos^3\theta\right), \tag{8}$$

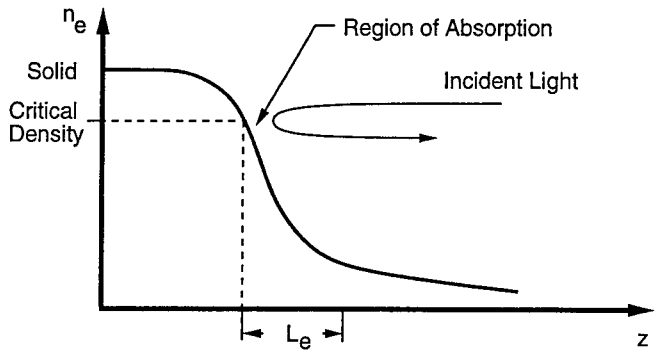

FIG. 7. Electron density versus position for a simple, one-dimensional, laser-heated plasma.

field to the plasma. The conditions under which resonance absorption or other higher-order processes are important are generally present only in laser inertial confinement fusion plasmas and will not be considered here.

The plasma electron temperature is determined by a balance between the absorbed laser energy and the loss of energy from the plasma. The primary loss mechanism is the conduction of energy to the colder, higher-density regions of the plasma near the target, which cannot be heated directly by the laser light. This cooling process is dominated by electron thermal conductivity, since the ion thermal velocity is much lower. Unfortunately, classical calculations of diffusive heat flow fail badly for the strong temperature gradients of laser-heated plasmas. Even with various extensions, they generally predict energy fluxes greater than $n_e E_T v_T$, where E_T and v_T are the electron thermal energy and velocity, respectively [37]. This is inconsistent, since diffusive energy flow must be limited to the product of the electron energy density times the thermal velocity. It is tempting to ascribe this breakdown to a transition to a collisionless energy transfer regime in which electrons free-stream rather than diffuse randomly, but experiments do not support this view. There is a large amount of experimental evidence covering a wide range of conditions that indicates that the heat flux in laser-produced plasmas is in fact well below the classical diffusive limit [41–45]. Despite extensive work, this anomalous inhibition of electron heat conduction is still not well understood, and no theoretical formulation is available. Reasonable fits to the experimental results, however, have been made by postulating a simple flux limit:

$$Q = f n_e E_T v_T, \tag{9}$$

where f is an empirical parameter that has been found to range from 0.03 to 0.1 over a wide variety of experimental conditions. This simplistic model is physically unsatisfying, yet little else is available. At the least, it is easy to apply.

different numerical factors [47]. Surprisingly, a number of different models all predict

$$T_e \propto (I_{abs}\lambda^2)^p, \tag{11}$$

where the exponent p varies between 1/4 and 2/3 [45].

To this point we have concentrated on electron processes and largely ignored the ions. Laser-produced plasmas are generally dense enough, at least in the hot radiating regions, to be considered in local thermodynamic equilibrium, with T_e determining the electron velocity distribution, the occupancy of excited states, and the ionization stage through the Maxwell velocity distribution, the Boltzmann formula, and the Saha equation, respectively. In addition, the energy equipartition time between electrons and ions is short enough, about a picosecond even for a 10-eV electron temperature, that T_e may be taken as the ion temperature as well. To first order, the distribution of ions will be peaked at the stage that has an ionization energy of a few T_e. Thus, a 15-eV plasma produced from a gold target will be dominated by Au^{+5} ions.

Radiation is emitted from laser-produced plasmas as electrons recombine with ions and decay downward through the various levels and ionization stages. High-atomic-number hot plasmas have many ionization stages with many radiating and absorbing levels that are highly broadened. They are optically dense over a broad spectral region, and the radiation is broad and relatively featureless. They are often characterized or modeled as a black-body radiator of temperature T_e, although the radiation does not rigorously obey Plank's law. Low-atomic-number plasmas necessarily have only a few ionization stages and are often optically thin except for the resonance lines. The resulting spectrum consists primarily of resonance line radiation with a low broad background. There have been many studies of the atomic number dependence of plasma spectra [10, 12, 14, 17, 48–52]. Figure 9 provides a useful summary: the conversion efficiency into several photon energy ranges is shown as a function of target atomic number. Although the curves have structure, the efficiency varies less than a factor of 3 for atomic numbers higher than 20. Extremely hot high-atomic-number plasmas can produce both broadband soft x-ray radiation from cooler regions, and K-shell and higher lines with kilovolt photon energies from hot highly ionized regions [53].

1.4 Practical Considerations

1.4.1 Targets

The simplest target is a bulk piece of the desired material in the form of a plate, disk, or rod. Since the spectrum or effective temperature of the source is only moderately dependent on target atomic number, at least for atomic numbers greater than about 20, the choice of target material is often determined by practical

experimental runs without requiring target renewal. Reasonable mechanical design must be used so that the target surface remains within the focal region as it moves so as to assure reproducible plasma formation. There is no evidence that special surface treatments improve plasma formation. Common machining techniques to achieve a reasonably flat surface and cleaning for vacuum seem adequate. (One exception to this is mentioned in the later section on short-pulse pumping.)

Other target configurations have been used for special applications. High-pressure gas [18] and gas jets [55, 56] avoid the problem of target replacement and are very clean. Liquid targets have also been used as self-renewing target surfaces [57]. Materials that are expensive or difficult to machine are often used in thin film form, either free standing or evaporated onto a plastic film. The film thickness can be adjusted so that the plasma just ablates through the film, providing radiation from both sides of the film [58]. Microcavities, several millimeters in diameter, have recently been studied as a way of producing true black-body radiators of very high temperature [59]. The laser is focused through a small hole and produces a plasma by heating a spot on the interior wall. Radiation from the plasma heats the entire interior wall, and subsequent reemission and absorption results in an intense thermal field with high uniformity obeying Planck's law. The complexity of the target, however, makes this a very low repetition rate source with low average output.

1.4.2 Focusing

Any focusing geometry that produces the required high power density is appropriate. Small focal spots reduce laser power requirements, but if the spot is very small, a few microns, the plasma density scale length, L_e, will be limited approximately to the spot radius and reduce the absorbed laser energy and plasma temperature. Similarly, for angles of incidence θ from normal, the light penetrates the plasma only to an electron density $n_C \cos^2 \theta$, and absorption and heating efficiency are reduced. If the experimental conditions require a high angle of incidence, special grooved target surfaces can be used to provide a local normal angle of incidence [60]. Single spot, multiple spot, and line foci have been used, formed by both refractive and reflective optics. Limiting the focal geometry to f-numbers greater than 10 reduces aberrations and allows simple uncorrected optics to be used.

1.4.3 Short-Pulse-Length Pumping

There are several advantages to using short-pulsed lasers for plasma generation. Damage and energy storage limitations force laser apertures and system cost to increase with pulse energy, usually much faster than linearly. Short-pulse excitation, therefore, offers a means of achieving the required high focal intensities for

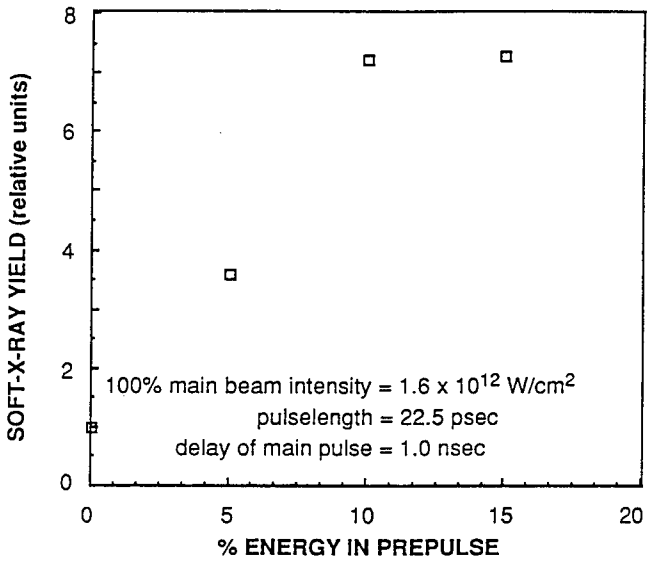

FIG. 11. Enhancement in plasma x-ray yield versus the fraction of main pulse energy used for the prepulse. From reference [63]. Reprinted with permission from the Optical Society of America.

for the prepulse. In these experiments the exact interval between the prepulse and the main pulse was not critical. Delays in the range of 1 to 2 nsec, corresponding to a plasma expansion of ~10 μm, were optimum. Experiments with very-high-intensity, 10^{17} W cm^{-2}, subpicosecond pulses yielded short optimum delays of about 20 psec [29]. In this parameter range, the coupling of plasma expansion, heating, and cooling processes are quite different.

Another approach to increasing efficiency when using ultrashort pulses is to use a target surface that has a built-in density gradient to reduce pump reflection. Etched microgrooves and colloidal porous coatings have been used successfully [64]. This technique increases the absorption of the pump laser energy into a plasma that is near solid density and results in high conversion efficiencies to x-rays above 1 keV energy.

1.4.4 Debris

Target material ablated by a laser-produced plasma ultimately is deposited on nearby surfaces. Laser-produced plasmas are effective evaporation sources and are frequently employed for vacuum deposition. In addition, small particles and droplets can be ejected from the target [65]. Thus, cell walls, windows, collection optics, gratings, etc., in the vicinity of the target will become coated with a thin

5. Fawcett, B. C., Gabriel, A. H., Irons, F. E., Peacock, N. J., and Saunders, P. A. H. (1966). *Proc. Phys. Soc. (Great Britain)* **88**, 1051.
6. Ehlers, A. W., and Weissler, G. L. (1966). *Appl. Phys. Lett.* **8**, 89.
7. Breton, C., and Popoular, R. (1975). *J. Opt. Soc. Am.* **63**, 1275.
8. Carroll, P. K., Kennedy, E. T., and O'Sullivan, G. (1978). *Opt. Lett.* **2**, 72.
9. Mahajan, C. G., Baker, E. A. M., and Burgess, D. D. (1979). *Opt. Lett.* **4**, 283.
10. Carroll, P. K., Kennedy E. T., and O'Sullivan, G. (1980). *Appl. Opt.* **19**, 1454.
11. O'Sullivan, G., Carroll, P. K., McIlrath, T. J., and Ginter, M. L. (1981). *Appl. Opt.* **20**, 3043.
12. Nicolosi, P., Jannitti, E., and Tondello, G. (1981). *Appl. Phys. B* **26**, 117.
13. Caro, R. G., Wang, J. C., Falcone, R. W., Young, J. F., and Harris, S. E. (1983). *Appl. Phys. Lett.* **42**, 9.
14. Orth, F. B., Ueda, K., McIlrath, T. J., and Ginter, M. L. (1986). *Appl. Opt.* **25**, 2215.
15. Gohil, P., Kaufman, V., and McIlrath, T. J. (1986). *Appl. Opt.* **25**, 2039.
16. Ginter, M. L., and McIlrath, T. J. (1986). *Nucl. Instrum. Methods A* **246**, 779.
17. Bridges, J. M., Cromer, C. L., and McIlrath, T. J. (1986). *Appl. Opt.* **25**, 2208.
18. Laporte, P., Damany, N., and Damany, H. (1987). *Opt. Lett.* **12**, 987.
19. Wang, J. C., Caro, R. G., and Harris, S. E. (1983). *Phys. Rev. Lett.* **51**, 767.
20. Benerofe, S. J., Yin, G. Y., Barty, C. P. J., Young, J. F., and Harris, S. E. (1991). *Phys. Rev. Lett.* **66**, 3136.
21. Kodama, R., Okada, K., Ikeda, N., Mineo, M., Tanaka, K. A., Mochizuki, T., and Yamakoshi, C. (1986). *J. Appl. Phys.* **59**, 3050.
22. Epstein, H. M., Schwerzel, R. E., Mallozzi, P. J., and Campbell, B. E. (1983). *J. Am. Chem. Soc.* **105**, 1466.
23. Lunney, J., Dobson, P. J., Hares, J. D., Tabatabaei, S. D., and Eason, R. W. (1986). *Opt. Comm.* **58**, 269.
24. Murnane, M. M., Kapteyn, H. C., and Falcone, R. W. (1990). *Appl. Phys. Lett.* **56**, 1948.
25. Sher, M. H., Mohideen, U., Tom, H. W. K., Wood II, O. R., and Aumiller, G. D. (1993). *Opt. Lett.* **18**, 646.
26. Nishimura, H., Matsuoka, F., Yagi, M., Yamada, K., Nakai, S., McCall, G. H., and Yamanaka, C. (1983). *Phys. Fluids* **26**, 1688.
27. Wood II, O. R., Silfvast, W. T., Macklin, J. J., and Maloney, P. J. (1986). *Opt. Lett.* **11**, 198.
28. Broughton, J. N., and Fedosejevs, R. (1992). *Appl. Phys. Lett.* **60**, 1818.
29. Külke, K., Herpers, U., and von der Linde, D. (1987). *Appl. Phys. Lett.* **50**, 1785.
30. Wood II, O. R., Silfvast, W. T., Tom, H. W. K., Knox, W. H., Fork, R. L., Brito-Cruz, C. H., Downer, M. C., and Maloney, P. J. (1988). *Appl. Phys. Lett.* **53**, 654.
31. Tom, H. W. K., and Wood II, O. R. (1989). *Appl. Phys. Lett.* **54**, 517.

53. Kauffman, R. (1991). "X-Ray Radiation from Laser Plasma," in *Physics of Laser Plasma*, A. Rubenchik and S. Witkowski (eds.), *Handbook of Plasma Physics*, Vol. 3, Chapter 3, pp. 111–162, North-Holland, Amsterdam.

54. Harris, S. E., and Kmetec, J. D. (1988). *Phys. Rev. Lett.* **61**, 62.

55. Charatis, G., Slater, D. C., Mayer, F. J., Tarvin, J. A., Busch, G. E., Sullivan, D., Musinski, D., Matthews, D. L., and Kippel, L. (1981). "Laser-Heated Gas Jet: A Soft X-Ray Source," in *Low Energy X-Ray Diagnostics—1981*, AIP Conference Proceedings, No. 75, D. T. Attwood and B. L. Henke (eds.), pp. 270-274, American Institute of Physics, New York.

56. Fiedorowicz, H., Bartnik, A., and Patron, Z. (1993). *Appl. Phys. Lett.* **62**, 2778.

57. Yamakoshi, H., Chin, C. T., Jaimungal, S., Herman, P. R., Budnik, F. W., Kulcsár, G., Zhao, L., and Majoribanks, R. S. (1993). "Extreme-Ultraviolet Laser Photo-Pumped by a Self-Healing Hg Target," in *Applications of Laser Plasma Radiation*, Vol. 2015, SPIE, Bellingham, WA.

58. Celliers, P., and Eidmann, K. (1990). *Phys. Rev. A* **41**, 3270.

59. Sigel, R. (1991). "Laser-Generated Intense Thermal Radiation," in *Physics of Laser Plasma*, A. Rubenchik and S. Witkowski (eds.), *Handbook of Plasma Physics*, Vol. 3, Chapter 4, pp. 163–198, North-Holland, Amsterdam.

60. Sher, M. H., Macklin, J. J., Young, J. F., and Harris, S. E. (1987). *Opt. Lett.* **12**, 891.

61. Tanaka, K. A., Yamauchi, A., Kodama, R., Mochizuki, T., Yamanaka, T., Nakai, S., and Yamanaka, C. (1988). *J. Appl. Phys.* **63**, 1787.

62. Weber, R., and Balmer, J. E. (1989). *J. Appl. Phys.* **65**, 1880.

63. Sher, M. H., and Benerofe, S. J. (1991). *J. Opt. Soc. Am. B* **8**, 2437.

64. Murnane, M. M., Kapteyn, H. C., Gordon, S. P., Boker, J., and Glytsis, E. N. (1993). *Appl. Phys. Lett.* **62**, 1068.

65. Silfvast, W. T., Richardson, M. C., Bender, H., Hanzo, A., Yanovsky, V., Jin, F., and Thorpe, J. (1992). *J. Vac. Sci. Technol. B* **10**, 3126.

66. Bortz, M. L., and French, R. H. (1989). *Appl. Phys. Lett.* **55**, 1955.

67. Powell, F. R., Vedder, P. W., Lindblom, J. F., and Powell, S. F. (1990). *Opt. Eng.* **29**, 614.

68. Catura, R. C., Joki, E. G., Roethig, D. T., and Brookover, W. J. (1987). *Appl. Opt.* **26**, 1563.

69. Ginter, M. L., and McIlrath, T. J. (1988). *Appl. Opt.* **27**, 885.

A Reasonably Practical XUV Laser for Applications

T. S. Clement, *Member, IEEE*, C. Tóth, J. Wu, and J. F. Young, *Senior Member, IEEE*

Abstract—**We describe a laboratory-scale 109 nm Xe Auger laser pumped by an all-commercial high-repetition-rate Nd:YAG laser system. The Xe laser provides pulse energies up to 1 μJ, and an average flux of 3×10^{12} photons/s at 11.5 eV. Measurements of the gain, output energy, and output beam shape are reported, along with an investigation of the time dependence of the gain.**

I. Introduction

THERE are many exciting applications of coherent extreme ultraviolet (XUV) sources in photochemistry, material science, atomic physics, and the life sciences, but to become practical, these applications require a convenient laser source that can be easily assembled and that can operate in the laboratory with a minimum of attention. We report a significant advance toward this goal: the first XUV laser system pumped by a standard, commercially available, Nd:YAG laser system at a high repetition rate. Gain in the XUV has been observed in several atomic species, including C [1], Cs [2], [3], Zn [4], Kr, and Xe [5], [6]. We chose to develop the Xe^{+2} Auger laser at 109 nm because of its unique combination of high gain, efficiency, benign physical properties, and short wavelength. In this paper we describe the construction of this source and present data on gain, output energy, and beamshape; initial investigations of the time dependence of gain are also reported.

The 109 nm Xe laser is pumped by soft X-rays from a laser-produced plasma through a process of inner-shell photoionization and subsequent rapid, selective Auger decay to the upper-laser level. Gains of about exp (7) were first observed in the Xe^{+2} Auger system using a 55 J, 1064 nm pump laser [5]. Subsequent optimization of operating parameters [7] and the development of new pumping geometries [8] resulted in an equivalent small-signal gain of exp (33), and a saturated output energy of 1 μJ using a 0.5 J pump laser [9]. Our present system achieves gains of about exp (25) and output energies of 1 μJ using a 250 mJ, ~ 100 ps pump pulse, the lowest pump energy reported for saturated output to date. This is also the highest-repetition-rate Xe Auger laser to date; it provides an average flux of 3×10^{12} photons/s at 11.5 eV.

Manuscript received September 24, 1993; revised January 19, 1994. This work was supported by the U.S. Air Office of Scientific Research. The work of T. S. Clement was supported by an IBM Graduate Fellowship.

T. S. Clement was with the Department of Electrical and Computer Engineering and the Rice Quantum Institute, William Marsh Rice University, Houston, TX 77251. She is now with Los Alamos National Laboratory, Los Alamos, NM 87545.

C. Tóth was with the Department of Electrical and Computer Engineering and the Rice Quantum Institute, William Marsh Rice University, Houston, TX 77251, on leave from the Research Institute for Solid State Physics, H-1525 Budapest, Hungary.

J. Wu and J. F. Young are with the Department of Electrical and Computer Engineering and the Rice Quantum Institute, William Marsh Rice University, Houston, TX 77251.

IEEE Log Number 9402503.

II. System Description

A schematic of the system is shown in Fig. 1. A Coherent Antares 76-s Nd:YAG CW mode-locked oscillator provides a 76 MHz train of ~ 100 ps long pulses at 1064 nm. A Continuum RGA-69 pulsed amplifier system is used to amplify selected pulses to an energy of about 250 mJ. The amplifier system consists of a regenerative amplifier stage followed by a single-pass 9 mm diameter Nd:YAG amplifier, all in a common housing. The amplifier system normally operates at a repetition rate of 10 Hz, but we have reduced the rate to 6 Hz because of the synchronization requirements of another experiment that also uses this amplifier. The entire pumping system occupies less than 2.5 m^2 of optical table space.

The 1064 nm pump beam is expanded to a diameter of about 2.5 cm and brought to a line focus on the plasma target using a cylindrical mirror at an ~ 83° angle of incidence. The several advantages of this grazing incidence geometry have been presented previously [8], [9]. The mirror, fabricated from BK7 glass, is 27.9 cm long × 7.6 cm high with a radius of curvature (concave) of 15.5 cm, and is coated with aluminum. Used at this steep angle, the mirror produces a line focus about 20 cm long, parallel to the mirror, about 127 cm away, the sagittal focal length. A cylindrical mirror, rather than a lens, was first used to pump the H_2 laser [10], and was later used for a Xe laser [11]. The mirror has lower aberrations than a lens at this angle, along with greater throughput, since the lens requires an antireflection coating that is difficult to design for this high angle of incidence. The lens coatings used in the past were absorbing, prone to damage, and very sensitive to polarization, wavelength, and angle of incidence. Current aluminium coatings can withstand fluences of about 50 $mJcm^{-2}$, and because of the large projected beam area on the mirror at this angle, we are about 10 times below that value. Nevertheless, contamination or dust can lead to damage, and it is important to protect the surface; we enclose the mirror in a plastic box with openings for the beams. A multilayer dielectric coat-

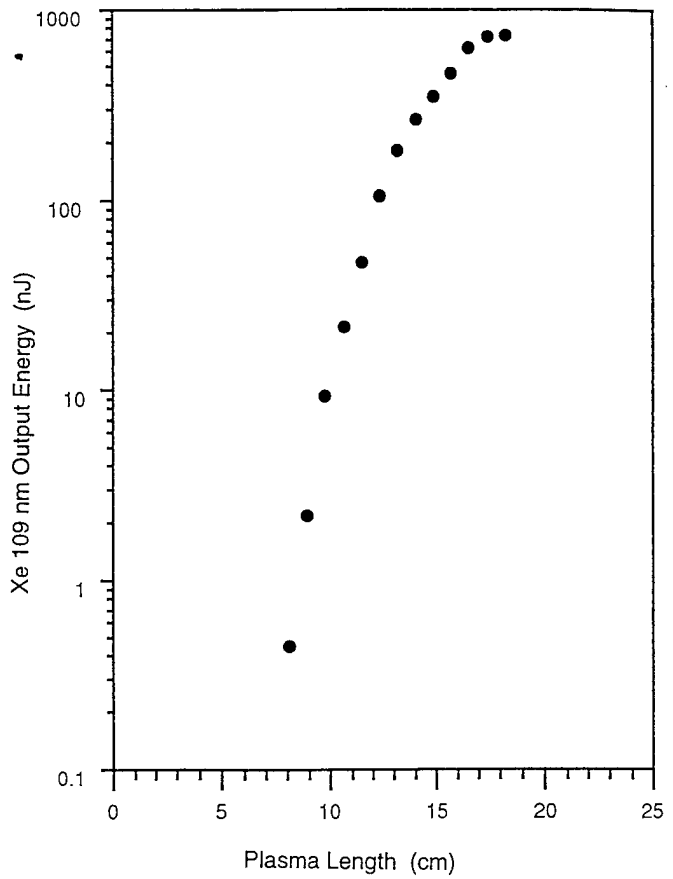

Fig. 2. Output energy versus pumped length for the 109 nm Xe Auger laser, for a Xe pressure of 14 torr.

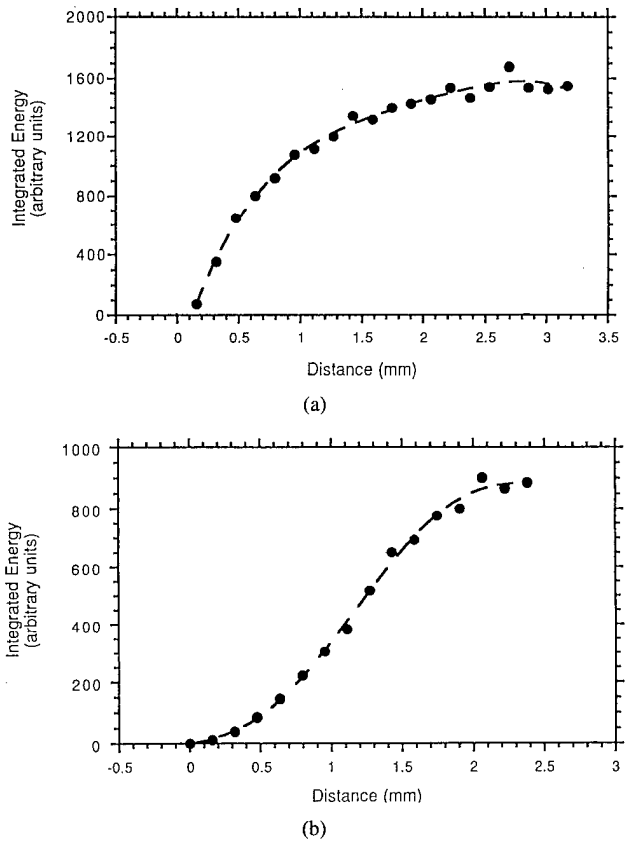

Fig. 3. Laser-beam energy transmitted past a scanning knife-edge, for a scan (a) normal to the target surface (horizontal), and (b) tangential to the target surface (vertical). The knife-edge was 80 cm from the front of the pumped region; the dashed curves are polynomial fits to the data.

ferent, in both cases the data indicate that 90 percent of the energy was transmitted through a 1.8 mm wide region. Thus, the output beam divergence in both planes was about 2.3 mrad, for a total solid angle of 16 μsr. At the output end of the pumped region, this solid angle corresponds to an effective emitting area of 8.1×10^{-3} cm^2, or a circle of 0.9 mm diameter. This result is consistent with the $\sim$ 1 mm absorption depth of the pumping soft X-rays from the laser-produced plasma into the surrounding Xe gas.

The lifetime of the Xe Auger 109 nm upper laser level has been measured to be 4.75 ns, with a collisional quenching rate of 2.8×10^7 torr$^{-1} \cdot$ s^{-1} [6], [13], [14]. This means that the lifetime should be longer than a nanosecond up to pressures of 28 torr, and that relatively long pumping pulse lengths should be effective in creating an inversion. (The lower laser level lifetime is calculated to be 8 to 10 ns, meaning the laser is self-terminating on our time scale.) Subsequent measurements of the time-integrated gain coefficient for various pumping pulse lengths, however, showed that the effective gain coefficient decreased for pumping-pulse lengths longer than a few hundred picoseconds, even for pressures of about 5 torr [7]. This suggests that other processes, probably electron collisions, reduce the effective inversion time under the experimental conditions normally used for lasers. To date, however, neither the exact nature of the competing process nor the time dependence of the gain have been determined. We investigated the time dependence of gain by dividing the pumping plasma into two regions: a 12 cm length to provide a probe beam, and a 3 cm long gain section to be measured. Fig. 4 shows the prism-beam delay arrangement that provided a variable time delay between the pumping of the gain region and the generation of the probe beam.

Fig. 5 shows the amplified probe output as a function of probe delay for two pressures. Each point on the graph represents the average of 20 measurements, yet the variability is still significant at low pressures where the signal levels are low, about ± 20 percent. Nevertheless, it is clear that the gain lifetime decreases with pressure, and is much shorter than predicted by collisional quenching alone. Quantitative conclusions, however, are difficult because the measured curves are convolutions of the gain decay function with the probe pulse shape. Sher measured the output pulse shape of a Xe system pumped with a 300 ps long pulse, both for unsaturated conditions—a total gain of exp (13)—and for saturated conditions, a gain of exp (40) [15]. The two cases were quite different; the unsaturated output pulse was symmetric in time with a width of 120 ps, while the saturated pulse was highly asymmetric and shortened to 50 ps. For all of our measurements, the probe region operated in the unsaturated

A better understanding of the gain dynamics might lead to several important improvements. A double-pass geometry would allow efficient energy extraction from the entire pumped volume, but our measurements indicate that the gain does not last long enough under our current conditions for this to be effective. Similarly, if excitation conditions could be found that would permit pumping with a Q-switched laser, considerable simplification of the pumping laser system would be possible. The method we used to measure the gain-time dependence had the advantage of simplicity, but it provided only limited information. We need to isolate the probe and gain regions so that we can control their parameters independently and explore lower pressure and excitation conditions.

REFERENCES

[1] S. Suckewer, C. H. Skinner, H. Milchberg, C. Keane, and K. Voorhees, "Amplification of stimulated soft x-ray emission in a confined plasma column," *Phys. Rev. Lett.*, vol. 55, pp. 1753–1756, 1985.

[2] C. P. J. Barty, D. A. King, G. Y. Yin, K. H. Hahn, J. E. Field, J. F. Young, and S. E. Harris, "12.8 ev laser in neutral cesium," *Phys. Rev. Lett.*, vol. 61, pp. 2201–2203, 1988.

[3] C. P. J. Barty, G. Y. Yin, J. E. Field, D. A. King, K. H. Hahn, J. F. Young, and S. E. Harris, "Studies of a 96.9 nm laser in neutral cesium," *Phys. Rev. A*, vol. 46, pp. 4286–4296, 1992.

[4] D. J. Walker, C. P. J. Barty, G. Y. Yin, J. F. Young, and S. E. Harris, "Observation of super Coster–Kronig-pumped gain in Zn III," *Opt. Lett.*, vol. 12, pp. 894–896, 1987.

[5] H. C. Kapteyn, R. W. Lee, and R. W. Falcone, "Observation of a short-wavelength laser pumped by Auger decay," *Phys. Rev. Lett.*, vol. 57, pp. 2939–2942, 1986.

[6] H. C. Kapteyn and R. W. Falcone, "Auger-pumped short-wavelength lasers in xenon and krypton," *Phys. Rev. A*, vol. 37, pp. 2033–2038, 1988.

[7] G. Y. Yin, C. P. J. Barty, D. A. King, D. J. Walker, S. E. Harris, and J. F. Young, "Low-energy pumping of a 108.9 nm xenon Auger laser," *Opt. Lett.*, vol. 12, pp. 331–333, 1987.

[8] M. H. Sher, J. J. Macklin, J. F. Young, and S. E. Harris, "Saturation of the Xe III 109 nm laser using traveling-wave laser-produced-plasma excitation," *Opt. Lett.*, vol. 12, pp. 891–893, 1987.

[9] M. H. Sher, S. J. Benerofe, J. F. Young, and S. E. Harris, "2-Hz 109-nm mirrorless laser," *J. Opt. Soc. Amer. B*, vol. 8, pp. 114–116, 1991.

[10] S. J. Benerofe, G. Y. Yin, C. P. J. Barty, J. F. Young, and S. E. Harris, "116 nm H_2 laser pumped by a traveling-wave photoionization electron source," *Phys. Rev. Lett.*, vol. 66, pp. 3136–3139, 1991.

[11] S. J. Benerofe, "Methods for efficient pumping of vacuum ultraviolet lasers," Ph.D. dissertation, Dep. Electr. Eng., Stanford Univ., Stanford, CA, 1991.

[12] C. E. Moore, *Atomic Energy Levels*, vol. III. Washington, DC: Nat. Bur. Standards, U.S. Gov. Printing Office, 1971.

[13] H. C. Kapteyn, M. M. Murnane, R. W. Falcone, G. Kolbe, and R. W. Lee, "Measurements on a proposed short wavelength laser system in Xe III," *Proc. SPIE*, vol. 688, Multilayer Struct. Lab. X-Ray Laser Res., N. M. Ceglio and P. Dhez, eds., pp. 54–59, 1987.

[14] H. C. Kapteyn, M. M. Murnane, and R. W. Falcone, "Time-resolved measurements of short-wavelength fluorescence from x-ray-excited ions," *Opt. Lett.*, vol. 12, pp. 663–665, 1987.

[15] M. H. Sher, "Techniques for short wavelength photoionization lasers: A 2-Hz 109-nm laser," Ph.D. dissertation, Appl. Phys. Dep., Stanford Univ., Stanford, CA 1989.

[16] H. Yamakoshi, C. T. Chin, S. Jaimungal, P. R. Herman, F. Budnik, G. Kulesár, L. Zhao, and R. S. Majoribanks, "Extreme-ultraviolet laser photo-pumped by a self-healing Hg target," *Proc. SPIE*, vol. 2015, Applicat. Laser Plasma Radiat., M. C. Richardson, ed., pp. 227–231, 1994.

[17] M. H. Sher and S. J. Benerofe, "Prepulsing of laser-produced plasmas for more efficient pumping of extreme-ultraviolet lasers," *J. Opt. Soc. Amer. B*, vol. 8, pp. 2437–2441, 1991.

T. S. Clement, photograph and biography not available at the time of publication.

Csaba Tóth was born in Hungary in 1959. He received the M.S. and Ph.D. degrees in physics from the Roland Eötvös University, Budapest, Hungary in 1983 and 1986, respectively. He has been working in the Research Institute for Solid State Physics of the Hungarian Academy of Sciences, Budapest, from 1983, where he is presently a senior scientific coworker. In addition he has been a Visiting Scientist at both the Research Center of Crete, Iraklion, Greece (1987, 1990) and Rice University, Houston, TX (1992/1993). His experience is connected with ultrashort light pulse generation, mode-locked solid-state lasers and investigation of multiphoton interaction processes at metal surfaces and soft X-ray excitation of ionic excimer molecules.

Dr. Tóth is a member of the Hungarian Physical Society, the SPIE, and the Quantumelectronics Division of the European Physical Society.

J. Wu, photograph and biography not available at the time of publication.

James F. Young is a Professor at Rice University in the Electrical and Computer Engineering Department. In addition to teaching undergraduate courses, he directs a research program concentrating on the development and application of extreme ultraviolet lasers, and on optical communications. Dr. Young received the B.S. and M.S. degrees in electrical engineering from the Massachusetts Institute of Technology in 1965 and 1966, and the Ph.D. degree in electrical engineering from Stanford University in 1970. In 1975 he was appointed Research Professor of Electrical Engineering at Stanford University, and taught graduate courses in lasers, directed graduate student research, advised undergraduates, and served in several administrative capacities. His research topics included optical parametric oscillators, nonlinear optics in crystals and vapors, infrared image upconversion, and the development of unique laser sources, including femtosecond, terawatt lasers. He joined the Rice University faculty in 1990.

Dr. Young is a Fellow of the Optical Society of America, a Senior Member of the Institute of Electrical and Electronic Engineers, and a member of Tau Beta Pi Engineering Honor Society. He received the Stanford Electrical Engineering Department Outstanding Service Award in 1985, and was named Stanford Master Advisor in 1988 in recognition of his service to undergraduates. He was chosen as an IEEE Lasers and Electro-Optics Society Distinguished Lecturer for 1991-92. He has authored over 70 publications, has served as a consultant to several companies, and has supervised the research of over 30 graduate students.

Optical gain in the ionic excimer $Cs^{2+}F^-$ excited by soft x rays from a laser-produced plasma

Cs. Tóth,* J. F. Young, and R. Sauerbrey

Department of Electrical and Computer Engineering and the Rice Quantum Institute, Rice University, Houston, Texas 77251-1892

Received August 5, 1993

Optical gain was observed on the $B \rightarrow X$ transition of the $Cs^{2+}F^-$ ionic excimer molecule at 185 nm. The excimer was produced by photoionization of CsF vapor with a laser-produced plasma source. An average net gain coefficient of 0.3 cm^{-1} was measured for 7 Torr of CsF and a 225-mJ pump laser.

We have observed gain in a new class of excimer molecule, the alkali halide ionic excimers. Soft x rays from a laser-produced plasma were used to photoionize CsF vapor and produce excited-state $Cs^{2+}F^-$, with an average gain coefficient of 0.3 cm^{-1} at 185 nm measured over a 6-cm length. To our knowledge this is the first demonstration of a new type of molecular ultraviolet laser with broad bandwidth and large saturation intensity.

The alkali halide ionic excimers are isoelectronic to the well-known rare-gas halides[1] and have emission wavelengths in the range from 210 to 130 nm.[2–4] The spectroscopy and kinetics of alkali halide ionic excimers were studied in detail by use of electron-beam,[5] ion-beam,[2,6] and soft-x-ray[3,4,7,8] excitation. A schematic potential energy curve for $Cs^{2+}F^-$ is shown in Fig. 1. Direct photoionization of the CsF ground-state molecule by soft x rays from a laser-produced plasma leads to the efficient formation of the $Cs^{2+}F^-$ (B) state,[4,7] which decays under emission of 185-nm radiation to the repulsive $Cs^{2+}F^-$ (X) state. The stimulated-emission cross section for this transition is estimated to be $\sigma = 2 \times 10^{-16}$ cm^{-2}.[1,9] Unlike the rare-gas halides, however, the ionic excimer precursor molecule CsF is slightly absorbing at the 185-nm excimer emission wavelength, with an absorption cross section of 3×10^{-18} cm^{-2}.[10] The primary products of CsF photoionization, however, have no measurable absorption at 185 nm, so the loss can be effectively eliminated with sufficient pumping flux. Detailed kinetic studies[9] predict a net gain of 0.2 cm^{-1} near a pumping source having a blackbody temperature of 20 eV for an initial CsF pressure of 3 Torr.

As discussed and demonstrated in Refs. 11–16, the oblique-incidence laser-produced plasma geometry has several advantages for efficient pumping of photoionization lasers. The spectral output corresponds approximately to a blackbody radiator with a temperature of 10–20 eV.[7,11,12,17] Long high-aspect-ratio excitation regions can be produced by use of moderate-energy pump lasers, and the traveling-wave plasma results in nearly synchronous excitation, which is important for short-lifetime upper levels. Our experimental setup is shown in Fig. 2. The plasma pumping source is a Nd:YAG-based mode-locked oscillator/regenerative amplifier system[16] that produces 225-mJ 100-ps 1064-nm pulses at 6 Hz. The beam diameter was enlarged to 3 cm and focused by a cylindrical mirror onto a stainless-steel plasma target rod inside a CsF heat-pipe cell. The mirror had a 60-cm concave radius of curvature, was coated with Al, and was used at a 60-deg angle of incidence relative to the normal, resulting in a 60-cm sagittal focal length and a 6-cm-long line focus. The laser intensity at the target surface was $\sim 3 \times 10^{10}$ W cm^{-2}. The target surface was grooved, as previously described, to produce a distributed series of pointlike plasma sources,[13–15] and it rotated continuously during the experiments.

The CsF vapor was produced in a heat pipe operating at temperatures as high as 850 °C. We estimate the CsF number density by measuring the vacuum ultraviolet absorption through the pumping region, using a laser-produced plasma point source at the end of the target rod. We compared the measured absorption in the region from 220 to 120 nm with previous data to determine the molecular density, assuming a uniform density along the length. The results were consistent (±20%) with the equilibrium vapor pressure corresponding to the cell temperature measured with external thermocouples.[10] CsF vapor pressures in the range of 1–10 Torr were used. He was used as a buffer gas to maintain the heat-pipe

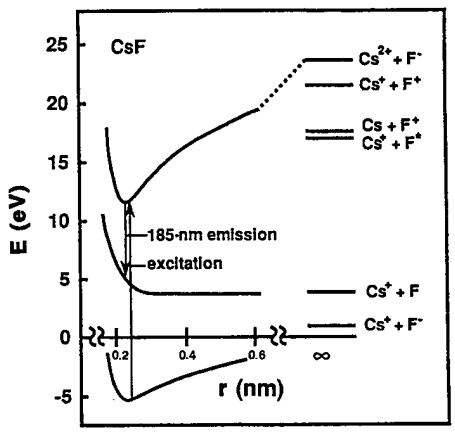

Fig. 1. Potential energy E versus internuclear separation r for the CsF ionic excimer.

0146-9592/93/242120-03$6.00/0

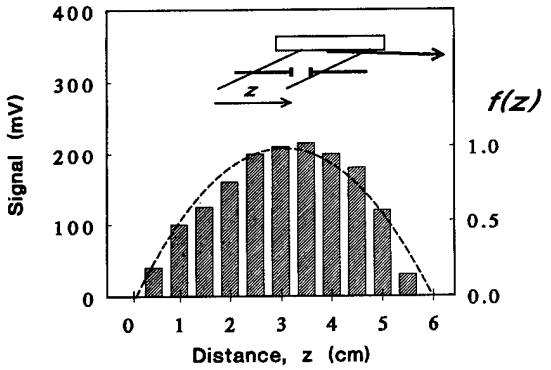

Fig. 5. Spatial distribution of 185-nm radiation along the excited region measured by scanning of a 0.5-cm aperture across the pumping beam. The dashed curve is a parabolic fit used to estimate the small-signal gain coefficients.

is the maximum excimer number density. Emission at the 240-nm reference wavelength showed the same dependence. Since the small-signal gain $g(z)$ is proportional to $n(z)$, the emission intensity, if we ignore constant atomic and geometrical factors, from an excited length z should be given by

$$I(z) \propto \exp\left[g_{\max}\int_0^z f(z')\mathrm{d}z'\right] - 1. \qquad (1)$$

An average gain coefficient for the total excited length L can be defined as

$$g_{\mathrm{avg}} = \frac{g_{\max}}{L}\int_0^L f(z)\mathrm{d}z = \frac{2}{3}g_{\max}. \qquad (2)$$

We determined values of $g_{\max}$ and g_{avg} by fitting relation (1) to the measured 185-nm emission signal. For a CsF pressure of 7 Torr, $g_{\max} = 0.44$ cm^{-1} and $g_{\mathrm{avg}} = 0.30$ cm^{-1}; at 4 Torr, $g_{\max} = 0.36$ cm^{-1} and $g_{\mathrm{avg}} = 0.24$ cm^{-1}. The solid curve through the 185-nm data of Fig. 4(a) is the best fit of relation (1). However, the emission intensity in the absence of gain, either at the reference wavelength or off axis at 185 nm, should be proportional to the simple integral $\int_0^z f(z')\mathrm{d}z'$. This function is plotted through the 240-nm data in Fig. 4(a) and for both curves in Fig. 4(b). In all cases there is good agreement between the measured points and the calculated curves.

As Fig. 3 shows, we also observed emission peaks at 158 and 161 nm. These signals were not present at the start of the experiment but grew in intensity in proportion to the number of plasma excitation pulses. The emission intensity remained approximately constant as the cell was cooled, reducing the CsF density to near zero. We attribute these peaks to the accumulation of F_2 in the interaction chamber. F_2 can be formed both directly from CsF photodissociation products and by means of $Cs^{2+}F^-$ (X) state dissociation following emission at 185 nm. The emission peak at 161 nm and the shift of the 158-nm peak from the well-known 157-nm F_2 laser line[18] can be attributed to vibrationally excited levels of the molecule in the high-temperature environment.

Molecular transitions typically have broader linewidths and lower stimulated-emission cross sections than their atomic counterparts. Although they require higher population inversions in order to reach the same gain, they also exhibit higher saturation intensities and output. The ionic excimers provide a welcome expansion of the available UV molecular laser lines. We have measured gain in $Cs^{2+}F^-$ that is consistent with theoretical predictions[1,9] and have demonstrated that substantial gain can be achieved with a moderately sized practical pumping system.

The authors take pleasure in acknowledging the important contributions of T. E. Sharp to the Nd:YAG laser system. We also thank S. E. Harris, G. Y. Yin, and C. P. J. Barty of Stanford University for the use of the heat-pipe cell and Tektronix for the donation of the transient digitizer. This research was jointly supported by the National Science Foundation, the U.S. Air Force Office of Scientific Research, the Robert A. Welch Foundation, and the OTKA Foundation of the Hungarian Academy of Sciences.

*Present address, Research Institute for Solid-State Physics, P.O. Box 49, H-1525, Budapest, Hungary.

References

1. R. Sauerbrey and H. Langhoff, IEEE J. Quantum Electron. **QE-21,** 179 (1985).
2. F. Steigerwald, F. Emmert, H. Langhoff, W. Hammer, and T. Griegel, Opt. Commun. **56,** 240 (1985).
3. S. Kubodera, L. Frey, P. J. Wisoff, and R. Sauerbrey, Opt. Lett. **13,** 446 (1988).
4. S. Kubodera, P. J. Wisoff, and R. Sauerbrey, J. Opt. Soc. Am. B **9,** 10 (1992).
5. T. T. Yang, V. T. Gylys, R. D. Bower, and D. G. Harris, J. Opt. Soc. Am. B **9,** 1272 (1992).
6. F. Steigerwald, H. Langhoff, and W. Hammer, J. Chem. Phys. **88,** 7376 (1988).
7. L. Frey, S. Kubodera, P. J. Wisoff, and R. Sauerbrey, J. Opt. Soc. Am. B **6,** 1529 (1989).
8. T. T. Yang, V. T. Gylys, and D. G. Harris, J. Opt. Soc. Am. B **6,** 1536 (1989).
9. S. Kubodera and R. Sauerbrey, Opt. Commun. **94,** 515 (1992).
10. S. Kubodera, P. J. Wisoff, and R. Sauerbrey, J. Chem. Phys. **92,** 5867 (1990).
11. S. E. Harris and J. F. Young, J. Opt. Soc. Am. B **4,** 547 (1987).
12. W. T. Silfvast and O. R. Wood II, J. Opt. Soc. Am. B **4,** 609 (1987).
13. M. H. Sher, J. J. Macklin, J. F. Young, and S. E. Harris, Opt. Lett. **12,** 891 (1987).
14. C. P. J. Barty, D. A. King, G. Y. Yin, K. H. Hahn, J. E. Field, J. F. Young, and S. E. Harris, Phys. Rev. Lett. **61,** 2201 (1988).
15. M. H. Sher, S. J. Benerofe, J. F. Young, and S. E. Harris, J. Opt. Soc. Am. B **8,** 114 (1991).
16. T. E. Sharp, Ph.D. dissertation (Rice University, Houston, Tex., 1993).
17. S. J. Benerofe, G. Y. Yin, C. P. Barty, J. F. Young, and S. E. Harris, Phys. Rev. Lett. **66,** 3136 (1991).
18. J. K. Rice, A. K. Hays, and J. R. Woodworth, Appl. Phys. Lett. **31,** 31 (1977).

Wavelength Encoding to Reduce Four-Wave Mixing Crosstalk in Multi-Wavelength Channels

Yile Guo, Behnaam Aazhang, and James F. Young
Electrical and Computer Engineering Department, Rice University
6100 Main Street, MS–366, Houston, Texas 77005; 713-527-4721, young@rice.edu

The trend toward higher bit rates in lightwave communications has increased interest in dispersion-shifted fiber (DSF) to minimize dispersion penalties. In addition, wavelength-division multiplexing (WDM) is being used to gain even greater capacity, and broad bandwidth erbium-doped fiber amplifiers are extending link distances between signal regeneration. Taken together, these techniques can result in severe performance degradation due to four-wave mixing (FWM) [1, 2, 3]. Several different ways of reducing the FWM degradation in WDM systems have been proposed, but all of the approaches increase system complexity and make it difficult to add channels to the system.

We show that wavelength-coded multiplexing can provide multiple channels on a simple fiber link while significantly reducing four-wave mixing interference compared to a WDM system. The FWM spectrum is symmetric and use of an antisymmetric code cancels the interference. Wavelength-coded multiplexing, also known as spectral code-division multiplexing (SCDM), has been proposed and demonstrated in optical fiber local area networks [4, 5, 6].

In a SCDM system each channel is assigned a combination of wavelengths (chips) as the channel's code, and the modulated signals of all channels are combined, propagate along the long-haul dispersion-shifted fiber, and experience attenuation and spectrum deformation due to FWM. Each receiver performs spectral correlation decoding with the same code as that of the corresponding transmitter, to pick out the desired signal and reject the signals from the other channels.

The key to good performance in a SCDM system is the orthogonality of the codes: the codes must have high autocorrelation and low crosscorrelation. A scheme for implementing truly orthogonal bipolar codes, as used in rf systems, in a noncoherent optical system has been proposed and experimentally demonstrated [4, 5]. To realize bipolar encoding/decoding in a unipolar system, a user k needs to send two sequences of unipolar codes $\mathbf{U}_k$ and $\overline{\mathbf{U}_k}$. $\mathbf{U}_k$ is obtained by replacing each -1 in the bipolar code with 0; $\overline{\mathbf{U}_k}$ is the complement of $\mathbf{U}_k$. The bipolar codes can be any orthogonal codes, say Walsh codes of length N. One way of sending the two distinct sequences is to concatenate them into one longer code, a form of wavelength multiplexing. There are many ways of concatenating $\mathbf{U}_k$ and $\overline{\mathbf{U}_k}$. The scheme we examine here is

$$\mathbf{U}_k \oplus \overline{\mathbf{U}_k} = \Big[U_k(1), U_k(2), \cdots, U_k(N), \overline{U_k(N)}, \overline{U_k(N-1)}, \cdots, \overline{U_k(1)}\Big], \quad (1)$$

where $\oplus$ represents concatenation. We denote the concatenated code for user k by $\mathbf{V}_k = [V_k(1), V_k(2), \cdots, V_k(2N)]$. This code can be called "antisymmetric" in the sense that it satisfies the relation: $V_k(i) = \overline{V_k(2N+1-i)}$, $i = 1, 2, \cdots, 2N$.

In the spectral domain, the encoding and decoding are implemented by dispersing the optical signal and filtering it with an amplitude mask in the wavelength plane. The pattern of the mask corresponds to the code. The transmitter for channel k encodes the signal according to the symbol source: $\mathbf{V}_k$ for bit "1" and $\overline{\mathbf{V}_k}$ for bit "0"; both $\mathbf{V}_k$ and $\overline{\mathbf{V}_k}$ are antisymmetric codes.

In channel k's receiver, the signal is split and correlated with the two complementary codes $\mathbf{V}_k$ and $\overline{\mathbf{V}_k}$. The decision statistic for channel k is given by the difference of the correlation signals detected by two photodiodes. This technique allows unipolar systems to implement the orthogonality of bipolar codes to reject signals from the other channels.

The FWM process destroys the orthogonality of the correlation detection and leads to crosstalk, i.e., the bits sent in other channels affect the decision statistic of channel k. In order to evaluate the performance of the SCDM system, we calculate the variation of the decision statistic caused by FWM in the fiber. The power spectrum at the input of the fiber, which is the sum of the power spectrum of the N users, is a random variable vector. The power in each chip is a random variable with a probability distribution that approaches Gaussian for a large number of users. The

Demonstration of All-Optical CDMA with Bipolar Codes

Tasshi Dennis, Behnaam Aazhang, James F. Young

Department of Electrical and Computer Engineering, Rice University
6100 Main Street, MS–366, Houston, Texas 77005; 713-527-4721, young@rice.edu

Abstract — **Using a fiber-based testbed, we experimentally verify that the advantageous correlation properties of bipolar spread-spectrum codes can be preserved in an optical channel using direct detection and all-optical encoder/decoders. The power spectrum of an erbium-doped superfluorescent fiber source is encoded, the codeword correlations are verified and rejection of multiple-access interference is demonstrated.**

I. Introduction

One of the challenges of fiber optic networks is to design methods of supporting a large pool of subscribers, not all of whom require access to the network at the same time, while providing access to many simultaneously active users. All-optical code division multiple access (CDMA) using bipolar codes developed for the radio-frequency domain is an attractive approach to meeting this challenge [1, 2, 3]. The primary problem is to design a coding technique that can preserve the advantageous correlation properties of bipolar codes using a direct detection, unipolar optical channel.

Our basic scheme has been reported previously [1]. In summary, for each length-N bipolar code X, we form a unipolar sequence U by replacing each -1 with 0. The unipolar super-code J of length $2N$ is then formed as the concatenation of U and its complement, $U \oplus \overline{U}$. In the same way, the bipolar code $-X$ can be transformed into the unipolar super-code $\overline{J} = \overline{U} \oplus U$, the binary complement of J. ON/OFF modulation of J and $\overline{J}$ forms the information symbols "1" and "0". The key to system performance depends on constructing a decoder that implements a true bipolar correlation using only unipolar signals and intensity detection. This can be accomplished using two unipolar correlations, followed by a subtraction [1]. Consider two bipolar codes X and Y and their super-codes $J = U \oplus \overline{U}$ (the pattern of light incident at the decoder) and $K = V \oplus \overline{V}$ (the pattern for receiving at the decoder). The zero-shift crosscorrelation of X and Y can be expressed as

$$\theta_{XY} = X \cdot Y = J \cdot K - J \cdot \overline{K}. \qquad (1)$$

The operations $J \cdot K$ and $J \cdot \overline{K}$ are unipolar correlations and therefore can be performed optically. In this paper, we present experimental results that demonstrate the effectiveness of this coding technique using a fiber-based system with modulated signals.

Our experimental apparatus performs spectral encoding and decoding of a superfluorescent fiber source (SFS) using a bulk grating and amplitude mask as shown in Fig. 1. At the encoder, portions of the spectrum transmited by the amplitude mask represent the super-code J, while portions reflected represent $\overline{J}$. At the decoder, the SFS input is replaced by the signal from the network channel, and the amplitude mask represents the super-code K. The two beams produced are therefore proportional to $J \cdot K$ and $J \cdot \overline{K}$. The decoder outputs are detected with a balanced receiver, so the resulting signal is proportional to the bipolar correlation θ_{XY}.

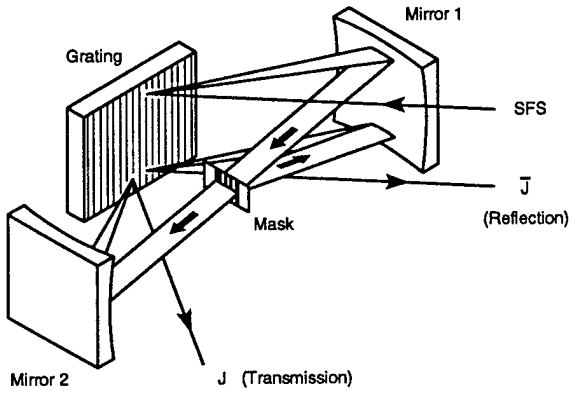

Fig. 1: The geometry for the grating based encoders. The spectral patterns of the two outputs, J and $\overline{J}$ are complements of one another, and are used to transmit a One and Zero respectively. The decoder has exactly the same geometry, but the SFS input is replaced by the signal from the network channel, and the outputs are focused onto a balanced receiver.

II. Experiment

Figure 2 shows a diagram of the experimental setup for these measurements. We used a SFS consisting of 40 m of highly doped erbium fiber pumped by a 150 mW, 980 nm pigtailed diode. About 22 mW of randomly polarized SFS power was divided with a fiber polarization splitter, forming broadband light sources for two encoders. We encoded about 9 nm of the bandwidth centered around the 1530 nm peak using Walsh codes. These codes, which have zero crosscorrelations in theory, were used to simplify comparison between theory and experimental results. Three codes of length N = 16, which we shall denote as super-codes J_A, J_B, J_C, and their complements, were etched on aluminum-coated glass substrates for each mask of the encoders and decoder in the testbed. The two outputs of each encoder, formed according to the selected bipolar code, are ON/OFF modulated with 2×1 interferometric optical switches according to the information symbol b. The modulated outputs are combined to form the network channel sent to the decoder. The mask of the decoder performs the bipolar correlation according to the code selected for receiving, and the output is detected with a balanced receiver and monitored with a spectrum analyzer.